

Temperature Induced Anomalous Exciton Localization in InGaN/GaN and GaN/AlInN Multiple Quantum Wells

By

Md. Soyaeb Hasan

A thesis submitted in partial fulfillment of the requirements for the degree of Master of Science in Engineering in the department Electrical and Electronic Engineering



Khulna University of Engineering & Technology
Khulna 920300, Bangladesh

August 2016

Declaration

This is to certify that the thesis work entitled " **Temperature induced anomalous exciton localization in InGaN/GaN and GaN/AlInN multiple quantum wells**" has been carried out by **Md. Soyaeb Hasan** in the Department of **Electrical and Electronic Engineering**, Khulna University of Engineering & Technology, Khulna, Bangladesh. The above thesis work or any part of this work has not been submitted anywhere for the award of any degree or diploma.

Signature of Supervisor

Signature of Candidate

Approval

This is to certify that the thesis work submitted by **Md. Soyaeb Hasan** entitled “**Temperature induced anomalous exciton localization in InGaN/GaN and GaN/AlInN multiple quantum wells**” has been approved by the board of examiners for the partial fulfillment of the requirements for the degree of **M.Sc. Engineering** in the Department of **Electrical and Electronic Engineering**, Khulna University of Engineering & Technology, Khulna, Bangladesh in August 2016.

BOARD OF EXAMINERS

1. _____ Chairman
Dr. Md. Rafiqul Islam (2) (Supervisor)
Professor
Department of Electrical and Electronic Engineering
Khulna University of Engineering & Technology

2. _____ Member
Dr. Ashraful Ghani Bhuiyan
Professor and Head
Department of Electrical and Electronic Engineering
Khulna University of Engineering & Technology

3. _____ Member
Dr. Md. Rafiqul Islam (1)
Professor
Department of Electrical and Electronic Engineering
Khulna University of Engineering & Technology

4. _____ Member
Dr. Md. Sherajul Islam
Assistant Professor
Department of Electrical and Electronic Engineering
Khulna University of Engineering & Technology

5. _____ Member
Dr. Anisul Haque (External)
Professor
Department of Electrical and Electronic Engineering
East West University, Dhaka, Bangladesh

Acknowledgement

All approvals belong to the Almighty ALLAH, the most kindhearted and bounteous to all His creatures and their actions. I humbly praise and grateful to Him, Who permits me to live and accomplish tasks including the research work being presented in this thesis.

The author gratefully express his deepest sense of gratitude and profound indebtedness to his thesis supervisor, **Dr. Md. Rafiqul Islam (2)**, Professor, Dept. of Electrical and Electronic Engineering (EEE), Khulna University of Engineering & Technology (KUET), Bangladesh, for his continuous supervision, encouragements, precious guidance, advices and helps, constructive criticisms and keen interests throughout the progress of the work. The author believes that work with him is a grand opportunity and would be a never-ending memory.

The author also extends his appreciation to Dr. Md. Sherajul Islam, Assistant professor, Dept. of EEE, KUET, Bangladesh. He brought me into a fantastic world of semiconductor optoelectronics. I learned from him that a qualified researcher should keep open mind and pay continuous effort. Without his valuable guidance and help, any success in this thesis work will never be possible. The author is also thankful to Prof. Takayuki Makino, Dept. of EEE, University of Fukui, Japan for his valuable discussion.

The author is grateful and expresses special thanks to Dr. Md. Rafiqul Islam (1), Professor, Dept. of EEE, KUET, Bangladesh, for his adorable attitude, precious mental support and lend a hand to make successful this thesis.

The author also gratefully acknowledges Prof. Dr. Ashraful Ghani Bhuiyan, Head, Dept. of EEE, KUET, Bangladesh, for providing all sorts of facilities to finish this work in time. The author is also indebted to all the teachers in the Dept. of EEE for their valuable counseling and constructive criticisms at every stages of the work, which helped him a lot to complete this study in time.

Last but not least, the author solemnly acknowledges his parents and all the family members, who gave him the utmost mental and financial supports throughout his whole student life and make a way to build up his career in the field of EEE.

August, 2016

Md. Soyaeb Hasan

Abstract


Temperature induced anomalous exciton localization in InGaN/GaN and GaN/AlInN multiple quantum wells

By Md. Soyaeb Hasan

InGaN and AlInN alloys including their relevant Quantum Well (QW) structures have attracted intensive research interest due to their potential applications in numerous optoelectronic devices. However, the emission mechanism in such QWs is still unveiled incompletely. The physical origin of spontaneous emission in InGaN/GaN or GaN/AlInN QWs is attributed to the recombination of localized excitons. The localization of exciton occurs due to the formation of Indium-rich clustering and abrupt interfaces between well and barrier layers. Conversely, the InGaN/GaN QWs can be grown without Indium-rich clustering and abrupt interfaces. Thus a detail understanding is essential to link the intricate structure of InGaN/GaN and GaN/AlInN QWs with their secretive optical behaviors.

In this dissertation, the details of exciton localization dynamics in InGaN/GaN and GaN/AlInN multiple quantum wells (MQWs) have been reported using Monte Carlo simulation of exciton hopping for a wide range of temperature of 10K to 300K. The calculated photoluminescence (PL) peak energy position of both of MQWs shows unusual behavior (redshift-blueshift-redshift) with the increase in temperature. The PL line width also exhibits W-shaped temperature dependent inhomogeneity. It is found that the phonon-induced lifetime variation of excitons have the remarkable effects on the PL peak position and line-widths in both of MQWs. The blue-shift of PL peak position is observed at high temperature in the MQWs with well and barrier thicknesses near the critical values, indicating the dominancy of two dimensional excitonic kinetics for the entire range of temperature.

Significantly, different temperature dependences for PL line-widths were perceived for the GaN/AlInN MQWs with different barrier heights. The MQWs having barrier height near to the lattice matched QW structure of GaN/AlInN showed the smaller band potential profile fluctuation. These results could be important to understand the emission properties of InGaN and AlInN MQWs optoelectronic devices.

Dedicated
To
My Beloved Parents

Respected Teachers

Contents

	PAGE
Title Page	i
Declaration	ii
Certificate of Research	iii
Acknowledgement	iv
Abstract	v-vi
Dedication	vii
Contents	viii-ix
List of Figures	x-xii
List of Illustrations	Xiii
Nomenclature	xiv
CHAPTER I Introduction and research objectives	1
1.1 Introduction	2
1.2 Motivation	3
1.3 Objectives	5
1.4 Synopsis of Dissertation	6
CHAPTER II Fundamentals of III-nitride QWs	7
2.1 Introduction	8
2.2 Crystal Structure of III-Nitride	8
2.3 Band structure of III-Nitride	9
2.4 Ternary alloys of III-Nitride	10
2.5 Exciton in III-nitride	11
2.5.1 Frenkel excitons	12
2.5.2 Wannier-Mott excitons	12
2.6 Quantum Well structure of III-Nitride	13
2.6.1 Multiple QW (MQW)	14
2.7 Photoluminescence (PL) studies	15
2.7.1 PL properties of direct-gap semiconductors	15
2.7.2 Effects of disorder	15
2.7.3 PL Spectra from MQWs	16
2.7.3.1 Peak energy of PL Spectra	17
2.7.3.2 FWHM of PL Spectra	17
2.8 PL study of III-nitride based MQWs	18
CHAPTER III Computational details	20
3.1 Introduction	21
3.2 Localized States in III-nitride QW structure	21
3.3 Density of localized states (DOS)	22
3.4 Exciton transport through disordered material	24

3.5	Monte Carlo simulation	27
3.5.1	Monte Carlo simulation of Exciton hopping	27
CHAPTER IV	Results and discussions	31
4.1	Introduction	32
4.2	Photoluminescence of InGaN/GaN MQWs	32
4.2.1	PL Peak energy in InGaN/GaN MQWs	35
4.3.2	PL line-width in InGaN/GaN MQWs	37
4.3	Optical properties of GaN/AlInN MQWs	39
4.3.1	PL Peak energy in GaN/AlInN MQWs	41
4.3.2	PL line-width in GaN/AlInN MQWs	42
CHAPTER V	Summary and outlook	44
5.1	Conclusion	45
5.2	Future Work	46
	Appendix	47
	Appendix A: Monte Carlo technique to calculate ‘pi’	47
	Appendix B: Derivation of DOS	49
	References	51

LIST OF FIGURE

Figure No	Description	Page
1.1	Band-gap energy of III-nitride semiconductor	2
1.2	A few important applications of III-nitride QW-based devices in current and future optical system	3
2.1	Wurtzite crystal structure of III-nitride semiconductor (AlN and GaN)	8
2.2	Wurtzite GaN band structure calculated by empirical pseudo potential calculations	9
2.3	Band-gap energy of III-nitride semiconductor	10
2.4	Schematic representation of exciton energy levels and an exciton in a semiconductor	11
2.5	Wannier-Mott exciton and Frenkel exciton in crystal structure	12
2.6	Schematic diagram (a) and ideal band structure (b) of single quantum well (SQW)	13
2.7	Schematic diagram (a) and ideal band structure (b) of multiple quantum wells (MQWs)	14
2.8	Schematic View (a) and typical photoluminescence spectra (b) from the Time Resolved Photoluminescence Spectroscopy (TRPL)	16
2.9	Temperature dependence of PL peak energy (a) and FWHM (b) for InGaN/GaN MQWs measured at different excitation powers	16
2.10	Temperature dependence of PL peak energy (a) and FWHM (b) for InGaN/GaN MQWs measured at different excitation powers	18
2.11	Schematic diagrams indicating the possible mechanism of carriers transferring in the MQWs structure.	19
3.1	Schematic view of band structure of typical III-nitride QW structure. Ideal structure is shown in Fig. (b), whereas the disorder induced band structures due to the internal alloy structure and imperfect interface are shown in Fig. (a) and Fig. (c), respectively.	21
3.2	(a) Potential profile fluctuation shown for three-period InGaN/GaN	22

	MQWs due to internal alloy structure and imperfect interface of well and barrier (b) Density of localized states with energy	
3.3	Gaussian distribution of the DOS with energy considering (a) localized states only and (b) both of localized states and delocalized states.	23
3.4	(a) Schematic plot of a disorder induced potential profile in InGaN alloy and (b) Gaussian DOS showing dispersion of the distribution of localized states within the cluster, σ and among the clusters, Γ	24
3.5	Typical III-nitride recombination paths.	25
3.6	Scheme of hopping transport through the disordered potential	26
3.7	Modeling for Monte Carlo simulation of exciton hopping in III-nitride MQWs.	27
3.8	Approximated flow chart to adopt Monte Carlo approach to simulate the exciton hopping and relaxation in III-nitride MQWs.	29
4.1	Photoluminescence spectra of InGaN/GaN MQWs for the temperature of (a) 10K and (b) 250K	32
4.2	Interrelation of Exciton energy (E_x), Band-gap energy (E) and the energy of emitted photon (E_0).	33
4.3	Calculated excitonic photoluminescence (PL) spectra of In _{0.22} Ga _{0.78} N/GaN MQW for the temperature range of 3-300K. The band peak positions are indicated by the dotted line. The horizontal axis is in units with respect to the exciton energy.	34
4.4	The photoluminescence peak energy positions for In _{0.22} Ga _{0.78} N/GaN MQWs with temperature. The dashed and dotted lines show the simulation results for traditional Monte Carlo simulation and the simulation results considering the temperature dependent variation of exciton lifetime, respectively. The solid line indicates the experimental temperature behavior of PL peak energy	35
4.5	Temperature dependent radiative lifetime of exciton in In _{0.2} Ga _{0.8} N/GaN MQWs. The thicknesses of well and barrier layer are 3nm and 4.3nm, respectively	36
4.6	The PL FWHM of photoluminescence bands for In _{0.22} Ga _{0.78} N/GaN MQW with temperature. The solid line shows the experimental FWHM. The dotted and the dash lines show the simulated FWHMs, for $\Gamma=0\text{meV}$	38

	and $\Gamma=29\text{meV}$ respectively.	
4.7	Schematic view of thirty period GaN/ $\text{Al}_{0.78}\text{Ga}_{0.12}\text{N}$ MQWs. The thicknesses of well and barrier layer are 1.5nm and 3.4nm, respectively.	40
4.8	Calculated excitonic photoluminescence (PL) spectra of $\text{InGaN}/\text{Al}_{0.78}\text{In}_{0.12}\text{N}$ MQWs for the temperature range of 3-300K. The band peak positions are indicated by the dashed line. The horizontal axis is in units with respect to the exciton energy.	41
4.8	(a) The peak energy positions of the photoluminescence (PL) bands for $\text{GaN}/\text{Al}_{0.88}\text{In}_{0.12}\text{N}$ MQWs with temperature. The solid line shows the experimental PL peak energies whereas the dashed line indicates the simulation results. (b) Temperature dependent PL peak energy position of $\text{GaN}/\text{Al}_{0.78}\text{In}_{0.22}\text{N}$ MQW.	42
4.9	(a) The FWHM for $\text{GaN}/\text{Al}_{0.88}\text{In}_{0.12}\text{N}$ MQW with temperature. The solid line shows the experimental PL FWHM whereas the dashed line indicates the simulation results. (b) Temperature dependence of FWHM of $\text{GaN}/\text{Al}_{0.78}\text{In}_{0.22}\text{N}$ MQW	43
A.1	Monte Carlo simulation approach to estimate the value of 'pi'.	47

LIST OF ILLUSTRATION

InN	Indium Nitride
GaN	Gallium Nitride
AlN	Aluminum Nitride
InGaN	Indium Gallium Nitride
AlInN	Aluminum Indium Nitride
AlGaN	Aluminum Gallium Nitride
IR	Infrared
UV	Ultraviolet
LED	Light Emitting Diode
QW	Quantum Well
MQWs	Multiple Quantum Wells
LASER	Light Amplification by Stimulated Emission of Radiation
PL	Photoluminescence
FWHM	Full Width at Half Maxima
CB	Conduction Band
VB	Valance Band
eV	Electron volt
QDs	Quantum Dots
LDs	Laser Diodes
CCD	Charged Couple Device
mW	mili-watt
meV	mili electron volt
DOS	Density of State
2D	Two dimensional

NOMENCLATURE

E_g	Band gap energy (eV)
c, a	Lattice parameter (nm)
x	Indium composition (%)
T	Temperature (K)
h	Plank's constant (J-s)
ν	Frequency (Hz)
E_{PL}	Photoluminescence Peak energy (eV)
E_x	exciton energy (meV)
E_0	energy of emitted photon (eV)
N	Concentration of localized states
α	Decay length of exciton wave function (nm)
τ_0	Radiative lifetime of exciton (ns)
ν_0	Attempt to escape frequency (Hz)
$D(E)$	Density of localized states
σ	Broadening parameter of DOS (meV)
Γ	Broadening parameter of DOS (meV)

Chapter

I

INTRODUCTION AND RESEARCH OBJECTIVES

Chapter at a Glance

- | | |
|-----------------------------------|--------------------|
| • Introduction | Section 1.1 |
| • Thesis Motivation | Section 1.2 |
| • Objectives | Section 1.3 |
| • Synopsis of Dissertation | Section 1.4 |

1.1 Introduction

Since a few years, III-nitride semiconductors and their alloys are of increasing scientific interest in the field of electronic and optoelectronic applications due to their wide direct band-gap tunability (Fig. 1.1) from Infrared (IR) to Ultraviolet (UV) region. Their direct energy band-gaps can produce light at high intensity which allow the fabrication of luminescence devices such as light emitting diodes [1] (LED) including visible and UV light (UV-LEDs), blue-UV lasers [2] with high external quantum efficiency. In modern era, numerous quantum structures of III-nitride semiconductors and their relevant alloys are intensively being studied because of their unique optical properties such as size-controlled tunable emission wavelength (known as the ‘quantum confinement effect’) and comparatively narrow emission spectra. All these attractive features have turned the III-nitride semiconductors as the excellent candidates for the development of next-generation display technologies. Moreover, due to the high absorption coefficient of III-nitride materials, they are widely used in solar to blind UV detectors [3]. Furthermore, they have attracted intensive research interest as the potentially valuable candidates in high-power electronics [4] due to their stabilities to high temperatures and good thermal conductivities.

To date, most of the III-nitride optoelectronic devices as shown in Fig. 1.2 are designed using InGaN/GaN or GaN/AlInN quantum well (QW) structures [5-8]. The QWs of these promising alloys facilitate us to fabricate the devices with optimized optical properties using band-structure engineering. However, the emission mechanism in such QWs is not still understood completely. The physical origin of spontaneous emission in InGaN/GaN or

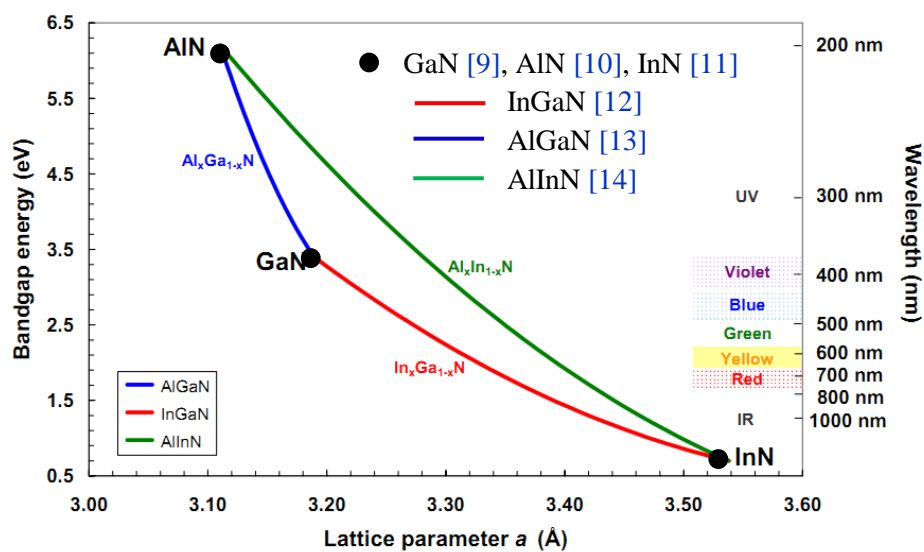


Figure 1.1: Band-gap energy of III-nitride semiconductor [15].

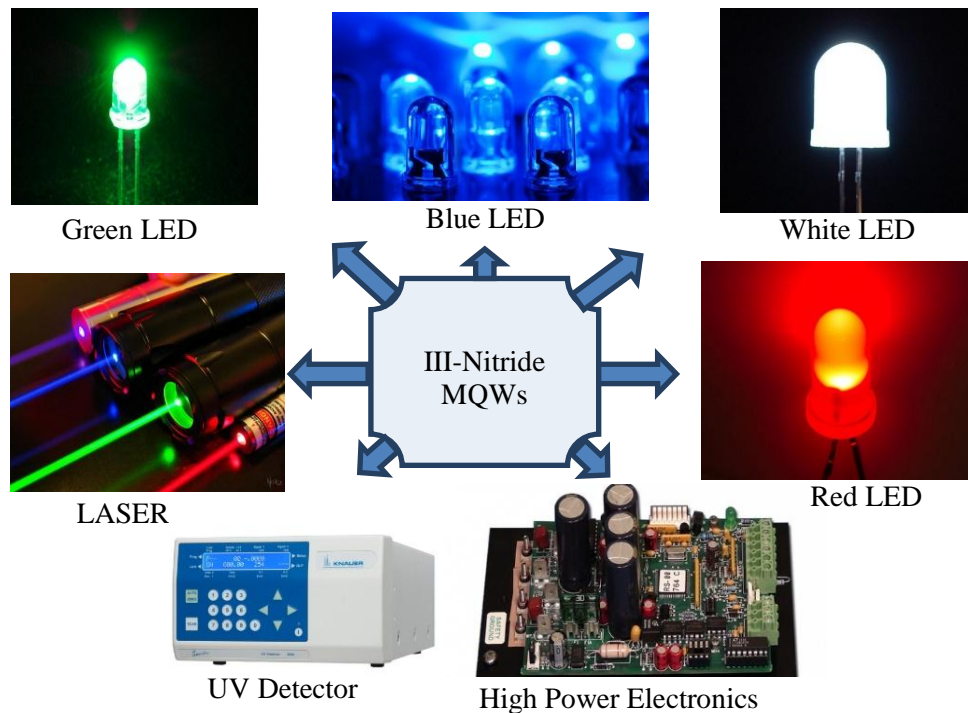


Figure 1.2: A few important applications of III-nitride QW-based devices in current and future optical system

GaN/AlInN QWs is attributed to the recombination of localized excitons [5, 6]. The localization of exciton occurs due to the formation of Indium-rich clustering and abrupt interfaces between well and barrier layers. Nonetheless, recent experiments [16] show that InGaN/GaN QWs can be grown without Indium-rich clustering and abrupt interfaces. Moreover, the nature of carrier and exciton motion and their distribution over the localized states with temperature remain a matter of dispute. A detail understanding is thus essential to link the intricate structure of InGaN/GaN and GaN/AlInN QWs with their secretive optical behaviors.

1.2 Motivation

Photoluminescence (PL) studies [5, 17-19] have widely been used to investigate the temperature behavior of emission characteristics in III-nitride QWs. An S-shaped (redshift-blueshift-redshift) temperature dependence [5] has been observed for the peak energy positions of PL spectra in InGaN/GaN multiple QWs (MQWs). Additionally, the W-shaped behavior of the PL line-widths is apparent with temperature [5]. These inhomogeneities in InGaN/GaN MQWs have been attributed to the exciton localization mechanisms. In contrast, the disappearance of the S- and W-shaped temperature behaviors has been reported in InGaN/GaN MQWs with increasing excitation power [17]. The reduced inhomogeneity

indicates the decreasing localization effect. More recent works [18, 19] have shown that semi-polar growth of InGaN/GaN MQWs reduces the Stoke's shift due to the significant reduction of piezoelectric field. However, the semi-polar growth of InGaN/GaN MQWs exhibits the stronger localization of exciton. Hence, the most experimental studies reveal the signature of exciton localization in InGaN/GaN MQWs either it is polar or semi-polar structure. Therefore, the knowledge of carrier localization dynamics with temperature is the key to investigate the anomalous behavior of emission characteristics in InGaN/GaN MQWs. Still now it is a great challenge to draw a universal conclusion about the temperature-induced carrier localization dynamics in InGaN/GaN MQWs.

For the qualitative explanation of the exciton localization mechanism i.e. the anomalous temperature behavior of the emission bands in InGaN/GaN MQWs, several studies [10, 13-15] have been performed including various types of models. The band-tail-filling model [17, 20] has been adopted to describe the recombination of localized exciton in InGaN/GaN MQWs. However, this model fails to explain the low temperature dynamics of exciton. Low temperature exciton localization mechanisms in InGaN/GaN QWs have been interpreted by numerical solutions of the effective mass Schrödinger equation [21]. This numerical approach has not successfully been applied for high temperatures exciton dynamics. Recent work [22] by Badcock et al. also reported the low temperature (10-100K) carrier redistribution dynamics in epitaxially grown InGaN/GaN QWs using the Monte Carlo simulation of phonon assisted exciton hopping. Meanwhile, the Monte Carlo simulation technique [5] has also been used to describe the inhomogeneous PL peak position and line-widths in InGaN/GaN MQWs for a wide range of temperatures. Although, the S-shaped behavior is visible from the experiment for the PL peak position, redshift is not found at high temperature from this simulation. Additionally, the simulated PL line-widths get saturated at high temperature, whereas the experiment shows that the line width increases ever more. Essentially, there is no quantitative description of the nature of exciton motion and their distribution over the localized states for a wider range of temperature in InGaN/GaN MQWs.

In addition, the research effort focusing the optical properties [7, 8] of GaN/AlInN QWs is still comparatively scarce than InGaN/GaN QWs. This is primarily due to difficulties with obtaining high-quality layers. Besides the wide band-gap tunability of AlInN alloy from IR to UV region, another important feature is the possibility to grow epitaxial layers which are lattice-matched to GaN at an indium content x of about 0.17 [23, 24]. It is worthwhile to point out that even in ideally lattice-matched GaN/AlInN QWs, in which piezoelectric polarization

is absent, large built-in electric field, can still be expected due to the spontaneous polarization properties of wurtzite crystals from the nitride family [25]. Furthermore, because of their higher structural quality, lattice-matched GaN/AlInN quantum wells (QWs) form an attractive alternative for the GaN/AlGaN system. Recent experiments [7] have revealed that GaN/AlInN QW heterostructure possess a considerable potential profile fluctuation and carrier localization. In contrast with InGaN/GaN QWs, band potential profile fluctuation exists in the barrier layers in the case of GaN/AlInN QWs which may influence the energy transition process. Thus it is urgently needed a phenomenological model describing quantitatively the exciton motion and their thermal distribution to explain the inhomogeneous PL peak energy and line width in InGaN/GaN and GaN/AlInN MQWs over a wide range of temperatures.

1.3 Objectives

The purpose of this dissertation is to go through systematically the details of the temperature-dependent localization dynamics of exciton i.e. the anomalous optical behaviors of PL peak energy and line-width in InGaN/GaN and GaN/AlInN MQWs. In order to calculate the PL spectra in both MQWs, the Monte Carlo Simulation of phonon-assisted exciton hopping and relaxation has to be performed considering additional inhomogeneous broadening with band potential fluctuation. The life time of exciton is affected by the phonon particle. The effect of temperature on the lifetime broadening of exciton has to be considered to simulate the hopping of exciton. This study also considers the thermal activation of exciton from localized states to delocalized states. The PL peak energies and the line widths have been calculated for the InGaN/GaN and GaN/AlInN MQWs with various Indium compositions over a wide range of temperature. In the course of this dissertation, the following objectives were achieved:

- (i) A quantitative model (using Monte Carlo simulation of phonon-assisted exciton hopping) is developed to explain the anomalous temperature behavior of emission spectra from InGaN/GaN and GaN/AlInN MQWs for a wide range of temperature.
- (ii) The PL peak energy position and the line-widths are calculated for InGaN/GaN and GaN/AlInN MQWs for the temperature range of 3K to 300K considering phonon-induced variation of exciton lifetime.
- (iii) The effect of barrier height on the temperature-induced inhomogeneous PL peak energy positions and line-widths has been investigated for GaN/AlInN MQWs.

1.4 Synopsis of Dissertation

This dissertation consists of five chapters mainly focusing on the inhomogeneous peak energy and line-widths of PL spectra in InGaN/GaN and GaN/AlInN MQWs for the temperature range of 3K to 300K. The brief summary for each chapter of this dissertation is as given below:

Chapter 1 provides the introduction of the study including potentiality of III-nitride MQWs in optoelectronic systems. The challenges in III-nitride MQWs towards the implementation of optoelectronic devices have been discussed. Thesis motivation and objectives of this thesis are also highlighted.

Chapter 2 focuses on the fundamentals of III-nitride MQWs as a potential candidate for current and future optoelectronic devices. Properties of InGaN/GaN and GaN/AlInN MQWs are analyzed to conduct the study.

Chapter 3 presents the Monte Carlo simulation technique to calculate the temperature-induced PL spectra from InGaN/GaN and GaN/AlInN MQWs. The incorporation of temperature-induced variation of exciton lifetime to conventional Monte Carlo simulation has been analyzed to calculate the peak energy position and line-width of the PL spectra.

Chapter 4 reveals the results of the study including the temperature-induced variation of PL peak energy position and line-width for InGaN/GaN and GaN/AlInN MQWs with various Indium compositions in the ternary alloys. Finally, for the precision of this model, the simulated results for PL peak energy position and line-width of both MQWs have been quantitatively fitted with experimental values for a wide range of temperature.

Chapter 5 concludes the outcomes of this thesis work and offers some suggestions which can serve as future problem areas for advance research in the field of InGaN/GaN and GaN/AlInN MQW-based optoelectronics.

Chapter

II

FUNDAMENTALS OF III-NITRIDE QWs

Chapter at a Glance

- | | |
|--|--------------------|
| • Introduction | Section 2.1 |
| • Crystal Structure of III-Nitride | Section 2.2 |
| • Band structure of III-Nitride | Section 2.3 |
| • Ternary alloys of III-Nitride | Section 2.4 |
| • Exciton in III-nitride | Section 2.5 |
| • Quantum Well structure of III-Nitride | Section 2.6 |
| • Photoluminescence (PL) studies | Section 2.7 |
| • PL study of III-nitride based MQWs | Section 2.8 |

2.1 Introduction

This chapter is intended to provide an introduction and overview of some important physical properties of III-nitride and their alloys. The basic physical properties such as the crystal structure and related defects, band structure, optical properties, carrier localization and hopping in disorder induced band structure of III-nitride based binary and ternary alloys have been derived that will be useful to understand the results in the later chapters.

2.2 Crystal Structure of III-Nitride

Binary group III-nitrides such as AlN, GaN, InN, TiN and their ternary and quaternary alloys possess a number of attractive physical, electrical and optical properties that allow the fabrication of novel materials and optoelectronic device structures [26]. The III-nitrides can crystallize in a hexagonal wurtzite as shown in Fig. 2.1 or in a cubic zinc blende crystal structure and cover a wide range of band-gap energies, depending on composition. The most stable crystalline structure of the III-nitrides is the hexagonal wurtzite crystal structure which is partially ionic due to large differences in the electronegativity of the group-III metal cations and nitrogen anions [27]. Due to the strong ionic III-nitride bonds, the unit cell is distorted from the ideal wurtzite structure, resulting in a large spontaneous polarization along the c-axis. The large differences in the ionic radii and bonding energies of the group-III metal cations give rise to different lattice constants, band-gap energies, electron affinities, which challenges the epitaxial deposition of the III-nitrides and its alloys. The lattice mismatch between the different III-nitride materials and commonly used substrates result in high dislocation densities, which impacts the mechanical and optoelectronic properties in the

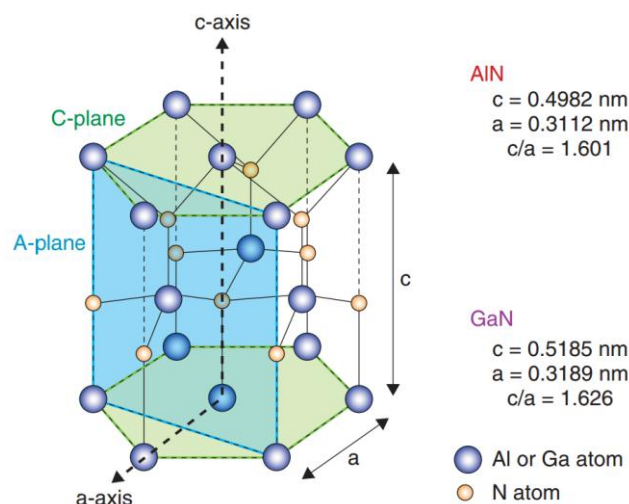


Fig. 2.1: Wurtzite crystal structure of III-nitride semiconductor (AlN and GaN) [28]

epitaxial layers [29]. Such imperfections also critically influence the surface morphology of heteroepitaxially grown III-nitride epilayers i.e. quantum well (QW) structures. Recently, due to advances in III-nitride native substrates, homoepitaxial and pseudo-morphic heteroepitaxial films with lower dislocation densities have been achieved that enhances the single and multiple QW based high efficient optoelectronic devices.

2.3 Band structure of III-Nitride

When an electron relaxes from the conduction band (CB) to valance band (VB) in a semiconductor, the band edge recombination can be direct or indirect. In a typical band structure an excited electron and hole will relax to the band edges to the minima in the CB and the maxima in the VB. If these points are vertically aligned in k-space, meaning they have the same momentum, recombination occurs in a direct mode and a photon can be emitted. If the minima in CB and maxima in VB do not align in k-space, a change in momentum is required before an electron and hole can recombine. This recombination is often assisted by a phonon, and the semiconductor is described as being indirect [30].

The III-nitride semiconductors are with direct band-gap Wurtzite band structure which is more complex, as can be seen in Figure 2.2 [31]. The allowed energy levels of electrons and holes form various maxima and minima, and crucially for GaN and related III-nitride alloys, the highest maximum and lowest minimum points are aligned, forming a direct band gap. Due to the direct band-gap of III-nitride semiconductor this material are of considerable interest now.

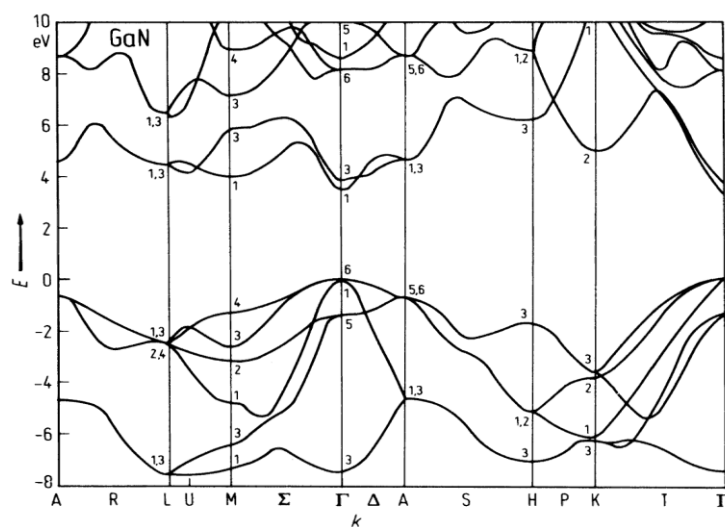


Figure 2.2: Wurtzite GaN band structure calculated by empirical pseudo potential calculations [31]

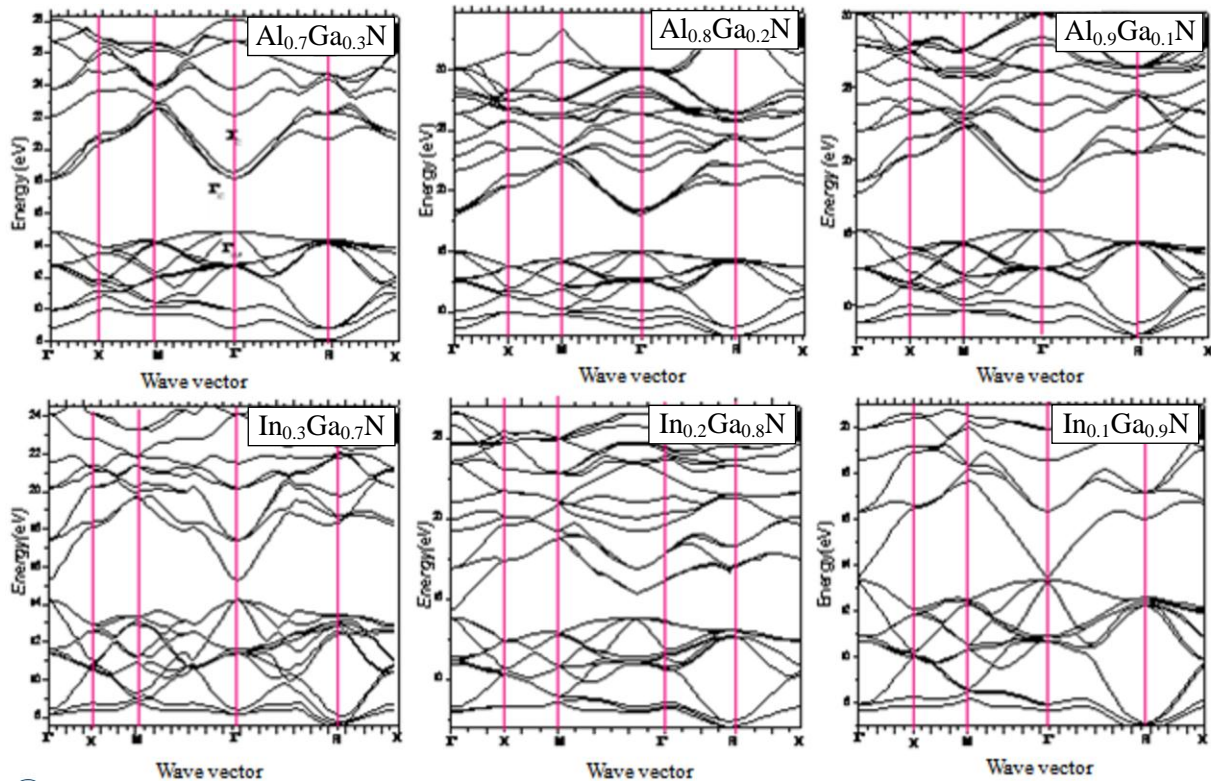


Figure 2.3: The band structure of InGaN and AlGaN ternary alloys estimated by ab initio calculation method [32]

2.4 Ternary alloys of III-Nitride

The III-nitride semiconductors have been recognized as promising materials for optoelectronic device application in the blue/green and ultraviolet wavelengths range due to their wide band gaps, ranging from 0.64 eV (InN) to 3.42 eV (GaN) and to 6.2 eV (AlN) [9-11]. The band-gap energy of III-nitride based ternary and quaternary alloy semiconductor can be engineered in theory to any value in this range, by incorporating different quantities of each constituent material [33]. With changing the composition of constituent element in the ternary/quaternary alloys, the band structure become more complicated due to the limited solubility to each other and some inheriting properties of III-nitride. The complicated band structures of InGaN and AlGaN ternary alloys have been shown in Fig. 2.3 as a function of Indium and Aluminium composition. Quaternary alloys can also be formed. However for the basis of this thesis ternary alloys are of considerable interest. The InGaN and AlInN alloys are widely being used in the production of optical emitters, where AlInN produces UV emitters with shorter wavelength than InGaN due to its higher band-gap, and InGaN produces emitters in the visible region with longer wavelength than the GaN band-gap. The band-gap energy of InGaN or AlInN can be calculated using Vagard's law [32].

2.5 Exciton in III-nitride

An exciton is a bound state of an electron and a hole which are attracted to each other by the electrostatic Coulomb force [34]. An exciton can form when a photon is absorbed by a semiconductor. The photon excites an electron from the valence band to the conduction band. In turn, this leaves behind a positively charged electron hole. The electron in the conduction band is then effectively attracted to this localized hole by the repulsive Coulomb forces from large numbers of electrons surrounding the hole and excited electron. This attraction provides a stabilizing energy balance. Consequently, the exciton has slightly less energy than the unbound electron and hole.

Excitons luminescence in semiconductor generally exhibits a narrow spectral line. The presence of free excitons usually indicates high crystalline of materials [35, 36]. In a direct band-gap semiconductor like III-nitride semiconductors, where the maximum of the VB and the minimum of the CB (as shown in Fig. 2.4) occur at the same value of the wave-vector, the energy of the emitted photon by free exciton recombination is [34]

$$h\nu = E_g - E_x \quad (2.1)$$

where E_g is the band-gap energy and E_x is the binding energy of the exciton.

The wave-function of the exciton is said to be hydro-genic [37]. However, the binding energy is much smaller and the particle's size is much larger than a hydrogen atom. This is because of both the screening of the Coulomb force by other electrons in the semiconductor (i.e., its dielectric constant), and the small effective masses of the excited electron and hole. The re-

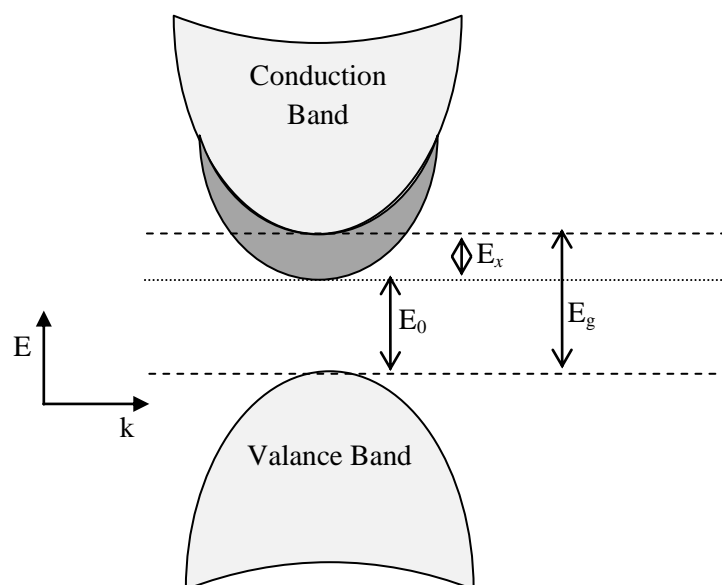


Figure 2.4: Schematic representation of exciton energy levels and an exciton in a semiconductor

combination of the electron and hole, i.e. the decay of the exciton, is limited by resonance stabilization due to the overlap of the electron and hole wave functions, resulting in an extended lifetime for the exciton. Depending on the properties of the material, excitons are classified in two types.

2.5.1 Frenkel excitons

The Frenkel exciton, named after Yakov Frenkel, has a typical binding energy on the order of 0.1 to 1eV. These excitons are typically found in alkali halide crystals and in organic molecular crystals composed of aromatic molecules, such as anthracene and tetracene. In this type of materials, there is a small dielectric constant, hence the Coulomb interaction between an electron and a hole may be strong and the excitons thus tend to be small. Typically the size of exciton is as same the size of the unit cell as shown in Fig. 2.5. Molecular excitons may even be entirely located on the same molecule, as in fullerenes.

2.5.2 Wannier-Mott excitons

This type of exciton was named after Gregory Wannier and Nevill Francis Mott. Wannier-Mott excitons are typically found in semiconductor crystals with small energy gaps and high dielectric constants. In semiconductors, the dielectric constant is generally large. Consequently, electric field screening tends to reduce the Coulomb interaction between electrons and holes which results in a radius larger than the lattice spacing as shown in

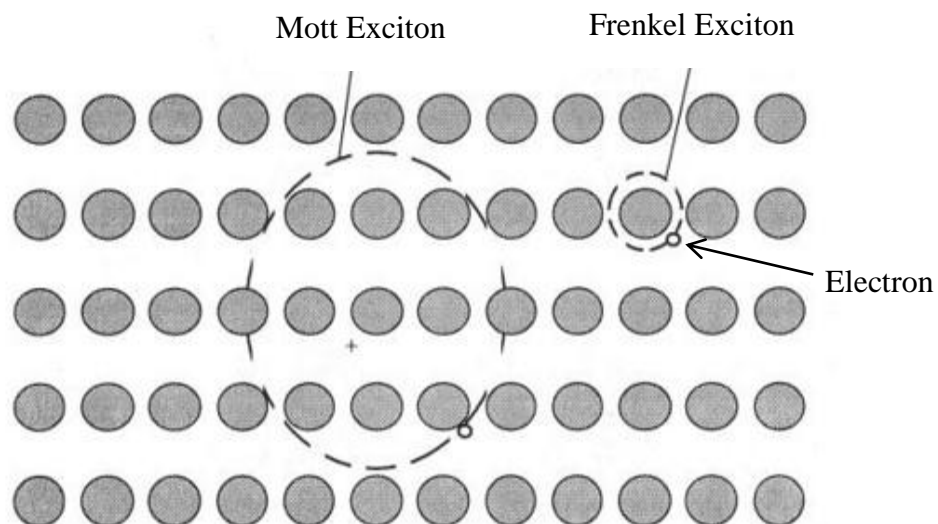


Figure 2.5 Wannier-Mott exciton, bound electron-hole pair that is not localized at a crystal position. Frenkel exciton, bound electron-hole pair where the hole is localized at a position in the crystal represented by black dots.

Fig.2.5. Small effective mass of electrons, typical of semiconductors, is also responsible for large exciton radii. As a result, the effect of the lattice potential can be incorporated into the effective masses of the electron and hole. Furthermore, due to the lower masses and the screened Coulomb interaction, the binding energy is usually much less than that of a hydrogen atom, typically on the order of 0.01eV.

2.6 Quantum Well (QW) structure of III-Nitride

With the development of semiconductor device technology, the improvement of LEDs and laser diodes has shown that heterojunctions and QWs are essential to achieve high external quantum efficiency. In these structures, the holes and electrons are injected in a small volume (QW) where recombination occurs more efficiently and with minimal losses. Figure 2.6 shows the InGaN/GaN QW structure where InGaN represents the well layer whereas the GaN as barrier layer. Akasaki and co-workers developed structures based on AlGaIn/GaN [38, 39] while Nakamura with great success exploited the combinations InGaIn/GaN and InGaIn/AlGaIn for producing heterojunctions, QWs and MQWs [40, 41]. In 1994, Nakamura and co-workers achieved a quantum efficiency of 2.7% using a double heterojunction InGaIn/AlGaIn [42]. With these important first steps, the path was cleared towards the development of efficient LEDs and laser diodes based on heterostructure QWs.

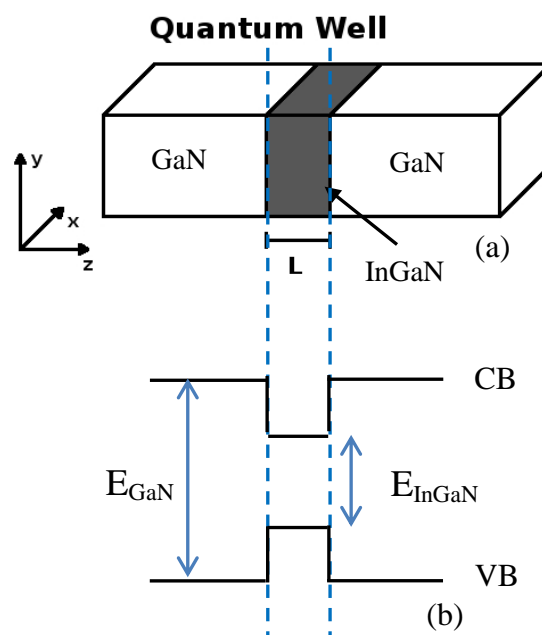


Figure 2.6: Schematic view (a) and typical band diagram (b) of InGaIn/GaN single Quantum Well (QW) structure

2.6.1 Multiple QW (MQW)

Multiple Quantum Wells (MQWs) are formed by repeating the same QW structure or by stacking the number of different QWs on the basis of application of this structure. The Fig. 2.7 shows the schematic diagram of a MQWs structure containing two repetitions of InGaN/GaN QW. MQWs are formed to improve the efficiency of optical device such as LED, LASER and light detecting devices etc. While increasing the Indium composition in InGaN layer for InGaN/GaN, the band-gap energy decrease. The band-gap energy of well layer is smaller than the barrier layer so that the carrier (exciton) can recombine (for light emitting device) or get absorbed (for solar cells) in the active layer.

However, in the Indium containing ternary alloy based MQW structure, with increase in Indium composition, the potential profile fluctuation increases indicating the inhomogeneous distribution of Indium [43]. But it has been reported the high external quantum efficiency of such QW based optoelectronic devices attributing the recombination of localized exciton [5, 6]. It is well known that the localized states formed by composition fluctuation acts as a Quantum Dots (QDs) which act as the radiative recombination center by retarding the carrier to go to the nonradiative centers such as dislocation and other defects. In this thesis, MQW structures of InGaN/GaN and GaN/AlInN have been considered to analyze the PL peak

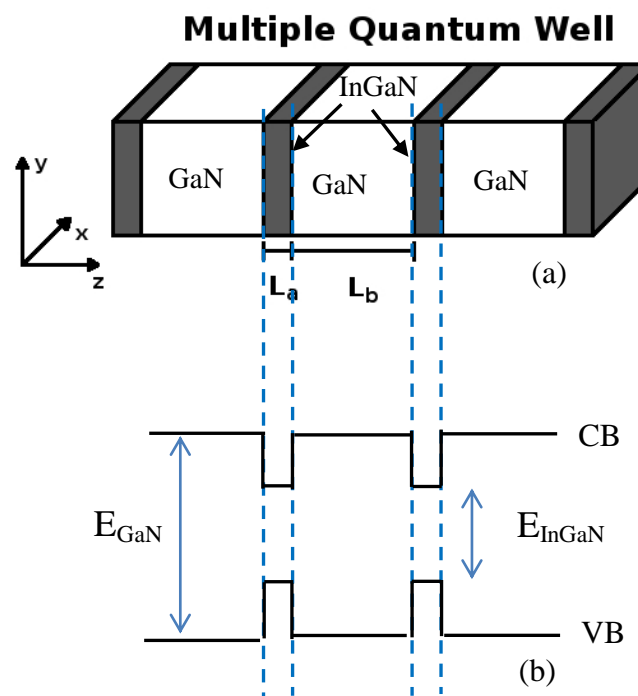


Figure 2.7: Schematic view (a) and typical band diagram (b) of InGaN/GaN Multiple Quantum Wells (MQWs) structure

energy position and line-width for wide range of temperatures. To analyze the effect of barrier height on the optical properties of MQW based light emitting device, two MQWs of GaN/AlInN with different barrier height have analyzed. PL study has been performed to observe the optical behavior in two different GaN/AlInN MQWs.

2.7 Photoluminescence (PL) studies

Photoluminescence (PL) is an efficient, sensitive and nondestructive tool to study the excited electronic states in semiconductors. It is an emission of radiation induced by the optical excitation of a sample under an external source of light. Laser light is the most widely used external excitation source for PL spectroscopy [44]. PL is an important technique to characterize specific information about semiconductors, particularly on structural imperfection and impurities [45]. Meanwhile, PL has been widely used in characterization of compound semiconductors.

PL spectroscopy is used for wide-ranging evaluations, including compositional analysis of the epitaxial layer of compound semiconductors, defect evaluation of light-emitting materials, evaluation of surfaces, non-destructive evaluation of integrated optical circuits, quantitative analysis of impurities, and evaluation of various LDs and LEDs.

2.7.1 PL properties of direct-gap semiconductors

In a typical PL experiment, a semiconductor is excited with a light-source that provides photons with energy larger than the band-gap energy. The incoming light excites a polarization that can be described with the semiconductor Bloch equations [46, 47]. Once the photons are absorbed, electrons and holes are formed with finite momenta k in the conduction and valence bands, respectively. The excitations then undergo energy and momentum relaxation towards the band gap minimum. Typical mechanisms are Coulomb scattering and the interaction with phonons. Finally, the electrons recombine with holes under emission of photons.

2.7.2 Effects of disorder

Real material systems always incorporate disorder. Examples are the structural [48] defects in the lattice or the disorder due to variations of the chemical composition. Their treatment is extremely challenging for microscopic theories due to the lack of detailed knowledge about perturbations of the ideal structure. Thus, the influence of the extrinsic effects on the PL is usually addressed phenomenologically [49]. In experiments, disorder can lead to localization

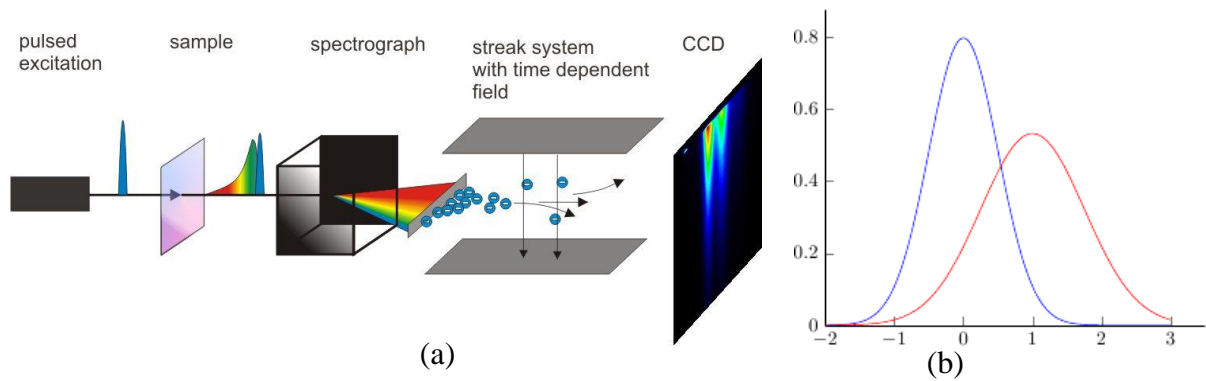


Figure 2.8: Schematic View (a) and typical photoluminescence spectra (b) from the Time Resolved Photoluminescence Spectroscopy (TRPL) [50]

of carriers and hence drastically increase the PL life times as localized carriers cannot as easily find nonradiative recombination centers as can free ones.

2.7.3 PL Spectra from MQWs

In photoluminescence (PL) technique, the sample is excited with light ('photo'). Some of the incident energy is emitted as light ('luminescence'), which implies the name PL. Excitation is usually by a laser, for convenience of directed beam, with beam power of 100's of mW. Laser light is absorbed by the crystal, exciting an electron from the valence band to the conduction band. In InGaN/GaN and GaN/AlInN MQWs, it is assumed that the PL spectra are obtained due to the recombination of localized exciton. There is pronounced effect of temperature on the PL peak energy position and line-widths.

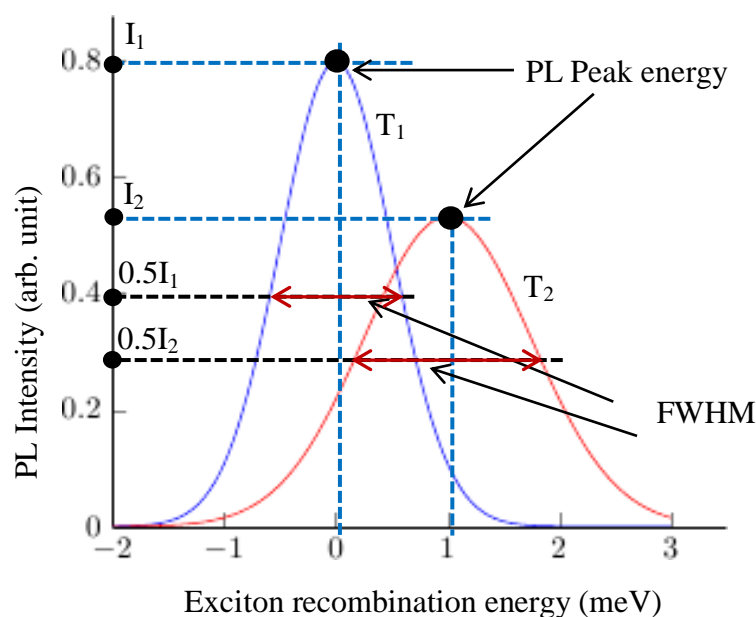


Figure 2.9: Luminescence spectra for two different temperatures.

2.7.3.1 Peak energy of PL Spectra

Generally the PL spectra are in Gaussian shape. In Gaussian shape there is peak position of the distribution which is the center of that distribution. For the case of PL spectra, when we obtain the PL intensity versus recombination energy curve as shown in Fig. 2.9, the peak position indicates that the maximum number of recombination occurs at that energy point. For this reason, the intensity is high at this energy point. In Fig. 2.9, there are two PL spectra which have been shown for two different temperatures. The PL peak energy changes with the change in temperature due to phonon-induced variation of exciton localization dynamics.

2.7.3.2 FWHM of PL Spectra

The FWHM or line-width is the width of the distribution at the point where the intensity (Y-axis) is half of the peak value. With change in temperature the PL intensity changes due to the reduction of radiative recombination of carrier in III-nitride based MQWs. In Fig. 2.9, for two different distributions, I_1 and I_2 are two different intensities have been indicated. The line-widths of each distribution are calculated using this I_1 and I_2 .

2.8 PL study of III-nitride based MQWs

Several experimental studies [5, 17-19] have been performed to investigate the PL behaviors in III-nitride MQWs structure. Some studies are performed to investigate the optical behavior for a particular temperature. Several studies are performed for low or high range of temperature. In this thesis, the temperature dependent PL behavior is investigated in InGaN/GaN and GaN/AlInN MQWs for the temperature range of 3K to 300K. Experimental studies reveal that the PL peak energy positions and the FWHM exhibit the S-shaped and W-shaped behavior with temperature as shown in Fig. 2.10 (a) and (b) respectively. Now question arises what are the reasons for such type of inhomogeneous behavior. Following explanation gives the possible mechanism for this type of inhomogeneity [17].

To explain in detail the above mentioned the S-shaped (W-shaped) temperature dependent behavior of the peak energy positions (line-width), the schematic diagrams shown in Fig. 2.11 indicate the possible mechanism of carriers transferring in the MQWs structure at different temperatures. At low temperature of (~6K), carriers are randomly distributed among the potential minima [Fig. 2.11(a)]. As the temperature increases from (up to 60K), weakly localized carriers are thermally activated and relax down into other strongly localized states

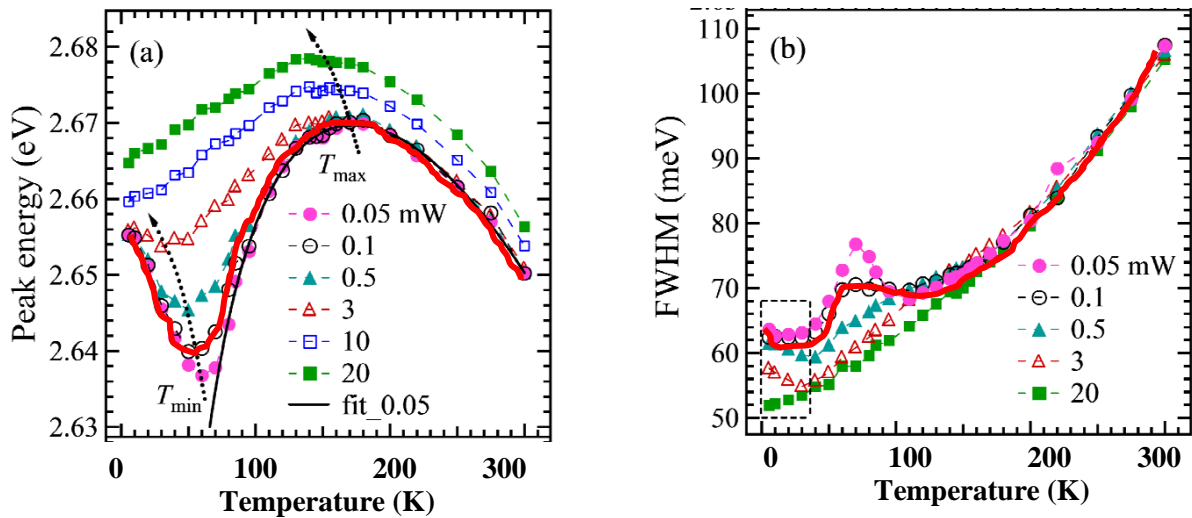


Fig. 2.10: Temperature dependence of PL peak energy (a) and FWHM (b) for InGaN/GaN MQWs measured at different excitation powers [17]

via hopping [49-52] and reach a saturated redistribution [Fig. 2.11(b)], which results in the initial redshift of the peak energy [Fig. 2.8(a)]. It is consistent with the initial decreasing of the PL line-width in the temperature range of $T \approx 6-40$ K [Fig. 2.10(b)]. After 60 K, increasing temperature enable carriers to achieve the thermal equilibrium with the lattice and to occupy higher-energy levels of the localized states [Fig. 2.11(c)], thus results in the blue-shift of the peak energy [Fig. 2.10(a)]. Accordingly, the rapid increase of the line-width in $T \approx 40-70$ K

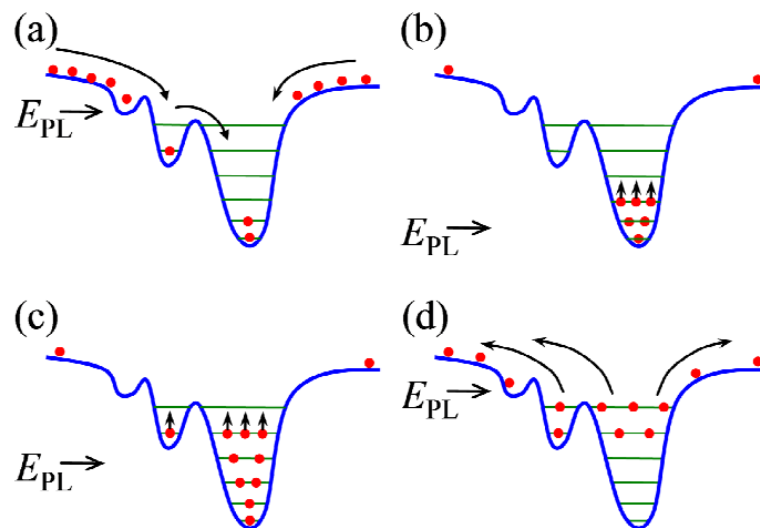


Figure 2.11: Schematic diagrams indicating the possible mechanism of carriers transferring in the MQWs structure. (a)-(d) represent respectively the case of the carriers distribution at lowest temperature (6K), lower temperature (60K), a slightly higher temperature (60-170K), and at higher temperature [17]

represents a crossover from nonthermalized to thermalized energy distribution of localized excitons [Fig. 2.10(b)] [5, 53]. A quick decrease of the line-width in $T \approx 70\text{--}110$ K as shown in Fig. 2.10(b), is explained as that when further increasing temperature above 70 K, even the most localized carriers become progressively mobile. Therefore the carrier distribution narrows [Fig. 2.11 (d)], and the line-width decreases. After $T \approx 110$ K, the role of the regular thermalization of carrier starts to become more and more important, which results in the line-width increase at a lower rate up to the full-delocalization temperature of $T_{\text{max}} \approx 170$ K [Fig. 2.10(b)]. It is consistent with the slow increase of the peak energy in the temperature range [Fig. 2.10(a)]. Finally, the peak energy decreases and the line-width increases markedly up to 300 K, in agreement with a regular thermalization of the carriers. Considering this physical mechanism of carrier transferring with temperature, the Monte Carlo simulation is performed for the exciton hopping which will be broadly discussed in the next chapter.

Chapter

III

COMPUTATIONAL DETAILS

Chapter at a Glance

- | | |
|--|--------------------|
| • Introduction | Section 3.1 |
| • Localized States in III-nitride QW structure | Section 3.2 |
| • Density of localized states (DOS) | Section 3.3 |
| • Exciton transport through disordered material | Section 3.4 |
| • Monte Carlo simulation | Section 3.5 |
| • Fitting Parameters in Monte Carlo simulation | Section 3.6 |

3.1 Introduction

This chapter clears the interfacing of the simulation technique to the physical origin of the inhomogeneous optical behavior in III-nitride MQWs. At first, the origination of localized states has been discussed. The distribution of localized states with energy has been analyzed. Finally, the transition of carrier (exciton) through the disordered QW structure has been calculated using the Monte Carlo simulation adopting the Millar-Abrahams rate.

3.2 Localized States in III-nitride QW structure

All the semiconductor heterostructures possess a certain degree of disorder due to the imperfect interfaces between the well and barrier layers as well as their internal alloy structure [49]. III-nitride QWs are the examples of heterostructures which are made by joining different materials, usually in layers, and with the materials joined directly at the atomic level. For InGaN/GaN or GaN/AlInN QWs, when two semiconductors are joined, it is not clear in advance how the different bands in the two materials will line up in energy with one another, and there is no accurate predictive theory in practice.

Due to the complex band structure as shown in Fig. 3.1 for wurtzite III-nitride semiconductors, there exists some localized states spontaneously [53]. The excitons recombine from these localized states and give luminescence. The Band structure of InGaN epitaxial layer is also more complicated due to the limited solubility of Indium into GaN matrix. However, the introduction of Indium into GaN plays a key role in strain and band

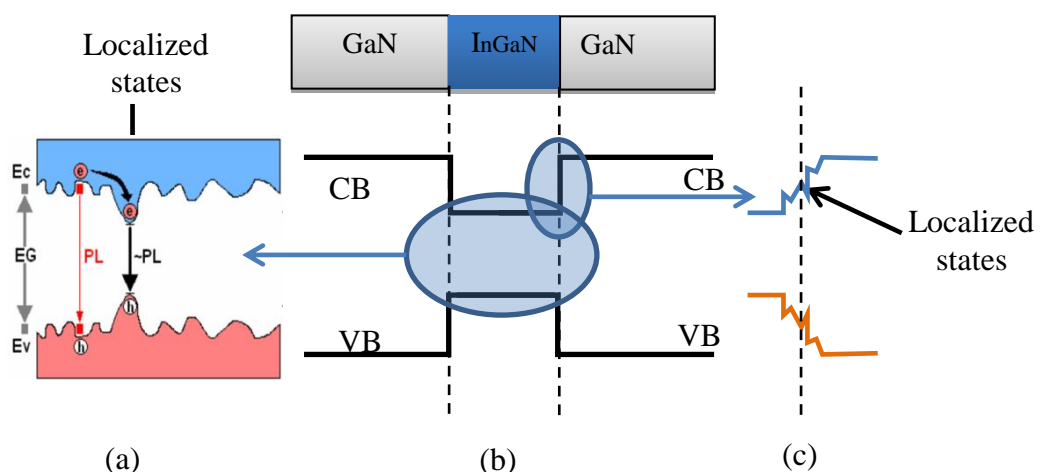


Figure 3.1: Schematic view of band structure of typical III-nitride QW structure. Ideal structure is shown in Fig. (b), whereas the disorder induced band structures due to the internal alloy structure and imperfect interface are shown in Fig. (a) and (c), respectively.

engineering of nitrides [54]. Indium is demonstrated to smooth the chaotic band-tail potential induced by partial disorder in the nitride alloys due to composition fluctuations [55]. In particular, in narrow QW's the interface roughness creates an essential disorder potential giving rise to band tails composed from localized states. These tails in general affect the dynamics of the Coulomb-correlated electrons and holes (exciton).

3.3 Density of localized states (DOS)

It is well known that an essential disorder potential in semiconductor heterostructures originates due to internal alloy structure and imperfect interfacing [49]. The disorder potentials give rise to band tails which are composed from localized states. These tails affect the dynamics of the Coulomb-correlated electrons and holes. In Fig. 3.2 (a), the disorder potentials with localized states are clearly visible. The density of localized states (DOS) is maximum near about the nominal value of band-gap energy of the well layer of MQW structure. With the decrease in energy below the conduction band (CB) of the well layer the DOS decreases. The reduction of DOS with energy as shown in Fig. 3.2 (b) could be in two ways viz. exponential or Gaussian. In the case of exponential distribution of DOS [49] with energy, the energy distribution of the localized states is given by:

$$g(E) = \frac{N}{E_0} \exp\left(\frac{E}{E_0}\right) \quad (3.1)$$

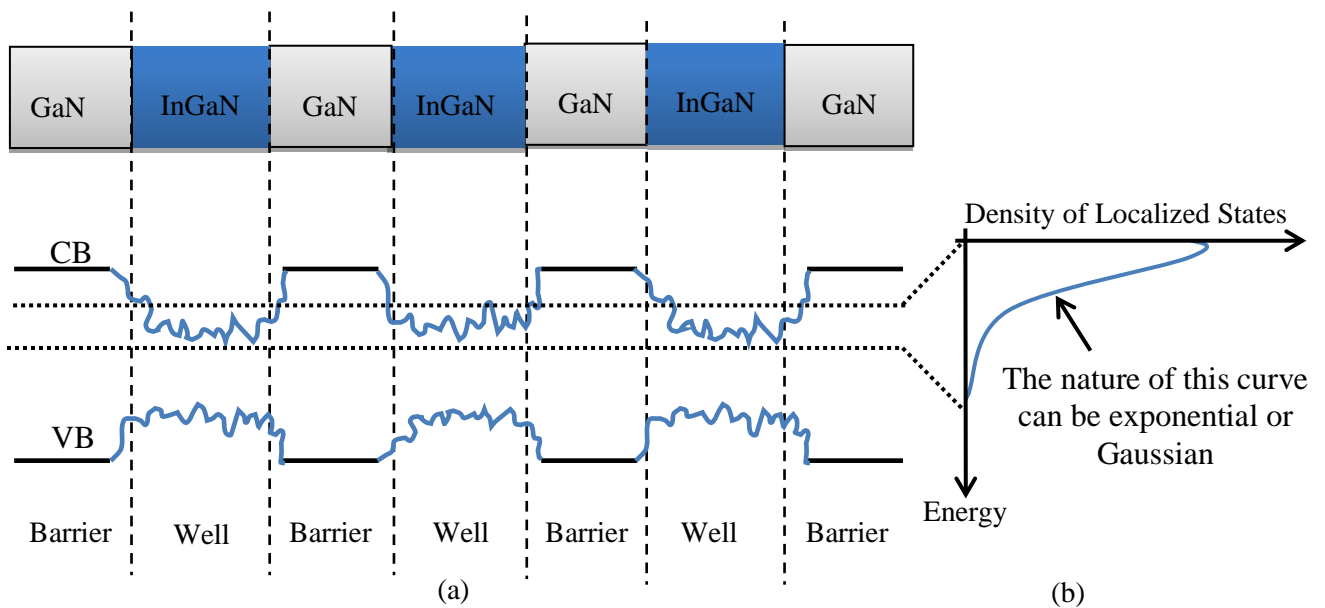


Figure 3.2 : (a) Potential profile fluctuation shown for three-period InGaN/GaN MQWs due to internal alloy structure and imperfect interface of well and barrier (b) Density of localized states with energy

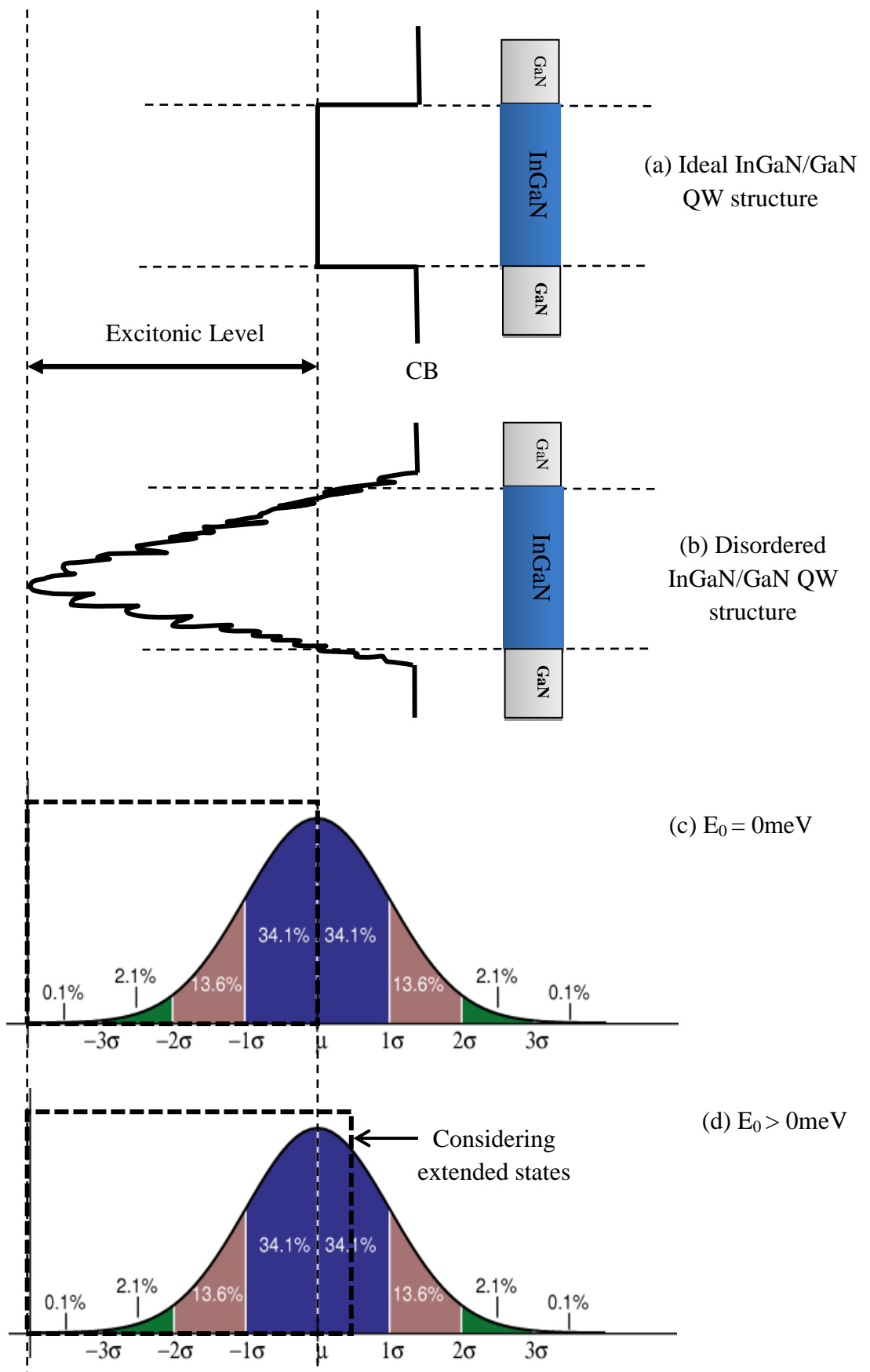


Figure 3.3: (a) Ideal and (b) disordered CB of InGaN/GaN QW. Gaussian distribution of the DOS with energy considering (c) localized states only and (d) both of localized states and extended states.

where N is the concentration of localized states and E_0 is the scaling energy. Normally it is considered that the reference energy, $E = 0$ which indicates the nominal band-gap energy of that material. In the case of Gaussian distribution of the localized states [49], a different mathematical expression than the exponential distribution gives the DOS which is given by the following expression,

$$g(E) = \left(\frac{N^2}{2\pi\sigma^2} \right)^{1/2} \exp \left[-\frac{(E - E_0)^2}{2\sigma^2} \right] \quad (3.2)$$

In this expression, N is the concentration of localized states and σ is the scale of the energy distribution. The reference energy is again $E = 0$, which is the middle of the distribution as shown in Fig. 3.3. Usually, all the energies in analyzing the excitonic phenomenon in III-nitride MQWs are considered below this value i.e. half distribution. The level of μ indicates the level of CB of the well layer. The rectangular window in Fig. 3.3 (c) shows the density of localized states only.

It has been assumed that, at high temperature, the thermal energy ($K_B T$) of carrier (exciton) is very high. Consequently there is a possibility of the carrier (exciton) to travel through the extended states and get recombined. This behavior is clearly visible in Fig 3.3 (b). If the extended states are considered to incorporate into the analysis exciton transition, some portion of the positive half of the Gaussian distribution is taken into account by setting some values of E_0 . The DOS considering the localized states as well as some portion of the extended states is depicted in Fig 3.3 (d) by a rectangular window (wider than the before rectangle).

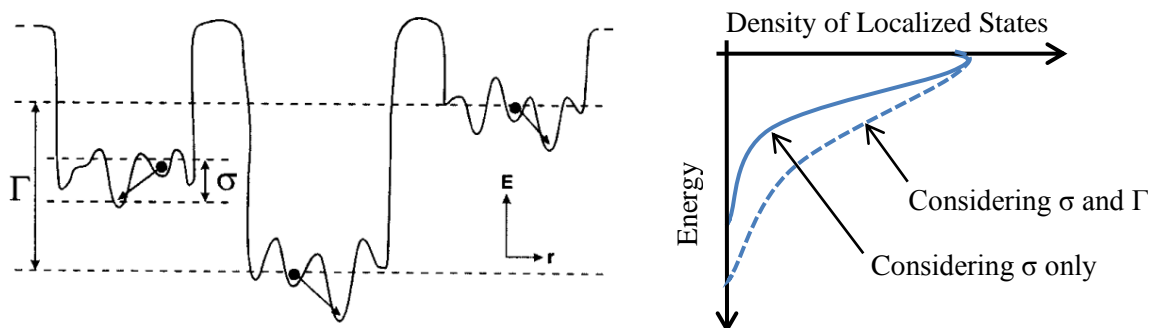


Figure 3.4: (a) Schematic plot of a disorder induced potential profile in InGaN alloy and (b) Gaussian DOS showing dispersion of the distribution of localized states within the cluster, σ and among the clusters, Γ [53].

In Gaussian distribution of DOS, σ indicates the potential profile fluctuation within the Indium-rich region for Indium containing ternary alloy based MQWs structure. Due to the phase separation in InGaN ternary alloy, different clusters originate with different Indium composition. The scale of energy distribution within the Indium-rich region and among the Indium rich region is not similar. To analyze the scale of energy distribution among the Indium rich regions additional scale Γ is incorporated to the σ as shown in Fig 3.4. Then the actual DOS [53] becomes (Appendix B):

$$D(E) \propto \exp\left[-\frac{(E - E_0)^2}{2(\sigma^2 + \Gamma^2)}\right] \quad (3.3)$$

3.3.1 Additional Inhomogeneity Parameter in Γ in III-Nitride MQWs

To calculate the numerical value of inhomogeneity parameter, σ (meV) in III-Nitride based MQWs, the experimental anomalous temperature behavior of PL line-width (FWHM) is carefully investigated. The experimental FWHM slightly increases at lower temperature whereas a sharp increase is observed at low temperature. At moderate range of temperature, the FWHM remains approximately constant whereas it increases at high temperature [5]. Therefore, the experimental FWHM shows the W-shaped behavior with temperature as shown in Fig. 3.5(a). Generally the value of inhomogeneity parameter, σ III-Nitride based QW structure is determined using the value of temperature at which the FWHM gets saturated. The temperature dependent value of σ can be estimated by the following expression [5],

$$\sigma(\text{meV}) = 2K_B T \quad (3.4)$$

In equation (3.4), the K_B is the Boltzmann's constant. The value of temperature at which the FWHM gets saturated is approximately 150K as shown in Fig. 3.5(a) which gives the dispersion parameter, $\sigma=25\text{meV}$.

The additional inhomogeneity parameter, Γ (meV) is strongly dependent on the Indium composition in the active layer of InGaN/GaN MQWs. The dependence of Γ on Indium composition in InGaN/GaN MQWs is given by the following linear fit with the experimental results [5] as shown in Fig 3.5 (b).

$$\Gamma(\text{meV}) = 360x - 50 \quad (3.5)$$

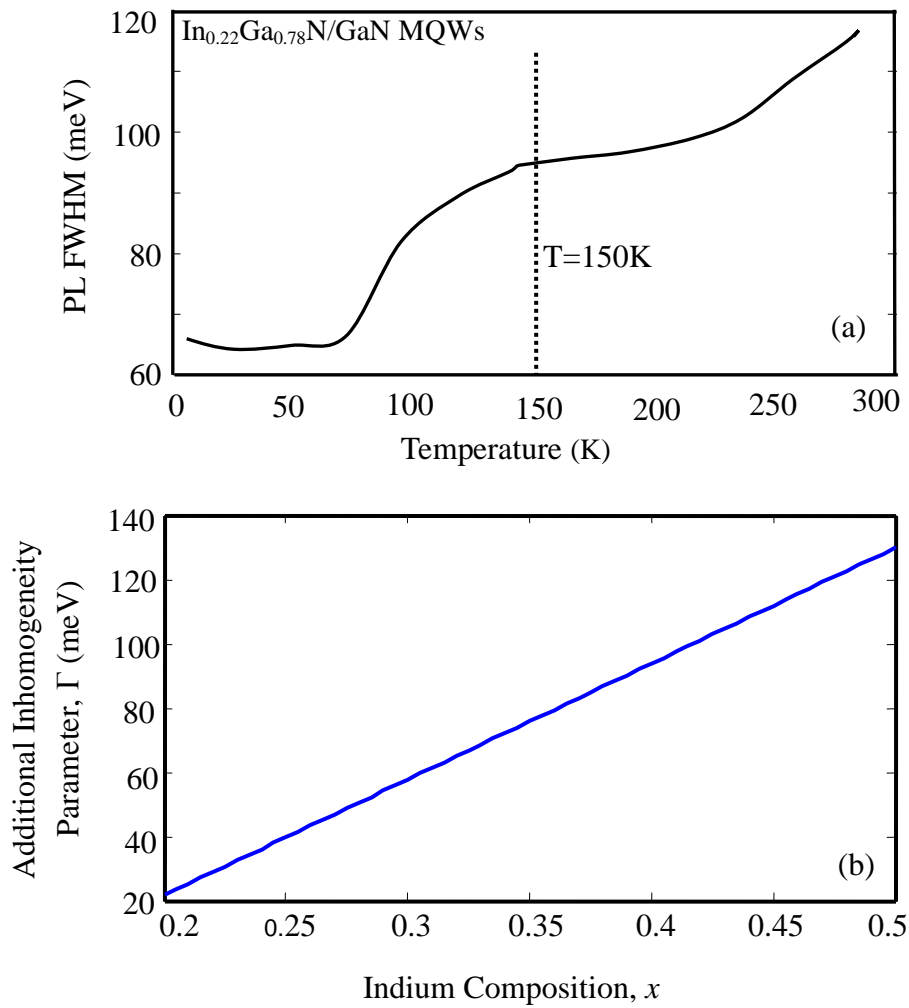


Figure 3.5: (a) The temperature dependent W-shaped PL FWHM for In_{0.22}Ga_{0.78}N/GaN MQWs [5] and (b) the composition dependent additional inhomogeneity parameter [5], Γ in InGaN/GaN MQWs

In equation (3.5), x is the Indium composition in the InGaN active layer of InGaN/GaN MQWs. It indicates that with the increase of Indium composition in InGaN/GaN MQWs, the formation of individual Indium-rich region increases.

3.4 Exciton transport through disordered material

The exciton created by the absorption of photon can recombine via several paths during the transport through the fluctuated band structure of III-nitride semiconductor. The separation of the electrons in the CB and holes in VB is broadly the band-gap of the semiconductor E_g . However, small changes in this energy result as the carriers occupy various points near the band edges of the band structure or recombine via mid band levels as shown in Fig 3.6.

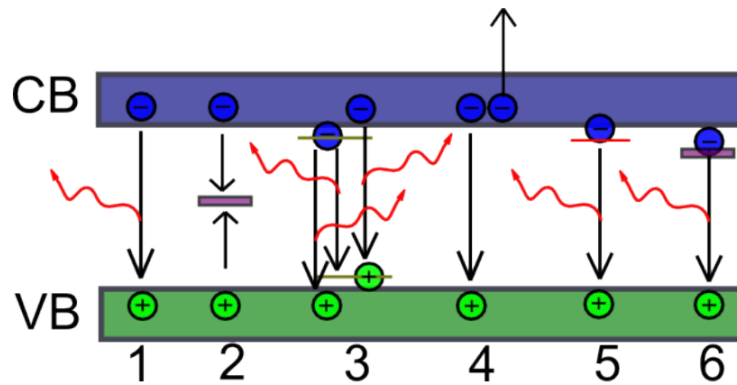


Figure 3.6: Typical III-nitride recombination paths [56].

Several recombination pathways exist for III-nitride MQWs as a result of the compositional fluctuation in ternary alloy and imperfect interfacing between well and barriers [33].

- (i) Path 1 is band to band recombination between electrons in the CB and holes in the VB, resulting in an emitted photon at the band gap energy of the material.
- (ii) Path 2 is a defect level transition, where the carriers recombine via a defect and lose energy non-radiatively (or by emission of a photon at much lower energy).

(either an electron higher up in the CB or a hole lower down in the VB) to a higher energy instead of emitting as a photon.

- (iii) Path 3 is emission related to dopants, either donor to acceptor emission, or frees to bounds. If the semiconductor material is doped, the dopant atoms may introduce a level below or above the CB and VB respectively. Recombination via these states results in a photon of lower energy than the original material band-gap.
- (iv) Path 4 is Auger recombination, and only applicable at large excited carrier density. The energy from a recombining electron and hole acts to promote a third carrier
- (v) Path 5 is exciton recombination, where an electron and hole are excitonically bound due to coulomb interactions. The excitons may be free to move through the structure, and recombine emitting a photon at slightly reduced energy.
- (vi) Path 6 is recombination via a phonon interaction, resulting in photon emission at a slightly reduced energy to the material band-gap.

Band-to-band radiative recombination, as path 1 in Fig. 3.6, results in a photon with the same energy as the band-gap, while the other paths result in a decrease in this energy, or lack of photon emission. In this thesis, exciton recombination, path 5 and path 6 is studied by measuring the PL peak energy position and line-widths for a wide range of temperature.

For a particular temperature, exciton recombination is a result of the Coulomb attraction between electron and hole. This increases the probability of an optical transition, and therefore the light emission efficiency in an III-nitride MQW structure. An exciton is a neutrally charged system of electron and hole bound together, with the ability to move freely in a semiconductor (allowing both electron and hole to remain coupled as they move) [57]. These free moving Wannier-Mott excitons may result in the majority of light emission from III-nitride MQWs. This is due to a high exciton binding energy in the III-nitride semiconductor [58]. The binding energy is calculated using Bohr model [59], where the large effective mass of an electron and hole in III-nitrides, and high dielectric constant of the semiconductor result in the large exciton binding energy.

While the PL spectra are observed for different temperatures, the recombination mechanisms of exciton change due to the phonon-assisted exciton hopping [53]. The exciton gets hop due to the interaction with the phonon particle. There are some possible fates of exciton as shown in Fig. 3.5. (I) Exciton gets radiatively recombine from a localized state by which the spectra

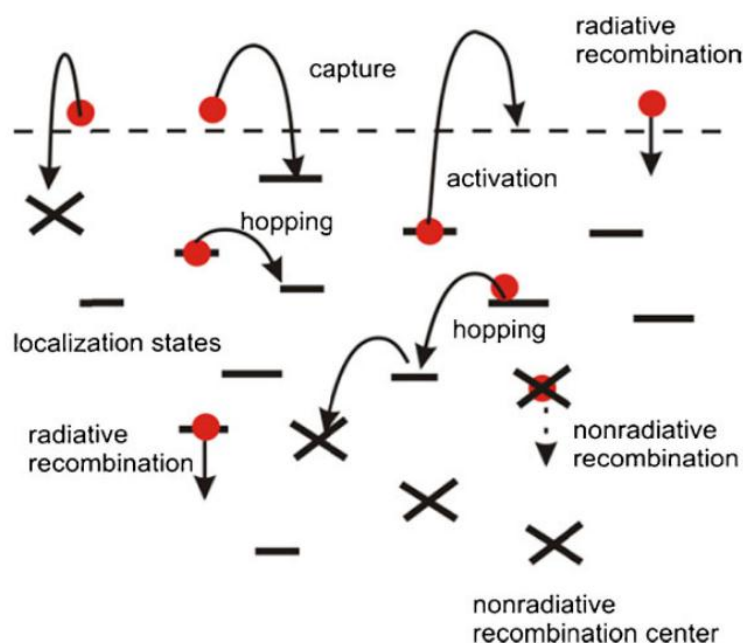


Figure 3.7: Scheme of hopping transport through the disordered potential [60].

of luminescence is observed. (II) Hopping of exciton may occur due to the interaction with phonon particle. By hopping exciton go to either a nonraditive center originated due to dislocation/other defects or another localized states giving luminescence. It is found that the hopping rate of exciton between the localized states is exponentially dependent on the distance and energy difference. The hopping rate between the localized states with energies E_i and E_j , respectively is given by Millar-Abrahams rate [61]

$$v_{ij} = v_0 \exp\left(-\frac{2r_{ij}}{\alpha} - \frac{E_j - E_i + |E_j - E_i|}{2k_B T}\right) \quad (3.6)$$

where, r_{ij} is the distance between localized states through which the hopping occurs, α is the decay length of exciton wave function, v_0 is the attempt to escape frequency in a localized state.

3.5 Monte Carlo simulation

The phonon-assisted hopping process of exciton as described in the previous section is attributed to the inhomogeneous optical behavior in InGaN/GaN and GaN/AlInN MQWs. Two possible phenomena are considered to explain the inhomogeneity in the MQW structures viz. (i) recombination of exciton and (ii) hopping of exciton. These two phenomena are simulated using Monte Carlo simulation technique [62]. The details of Monte Carlo simulation technique have been illustrated in Appendix.

3.5.1 Monte Carlo simulation of Exciton hopping

The simulation technique to study the hopping energy relaxation and luminescence of excitons is similar to that suggested by Silver et al. [63, 49]. It is assumed that excitons behave like single particles in their hopping movement between localized states. However, contrary to single electrons and holes recombining via tunneling processes, excitons have some typical lifetime τ_0 with respect to their radiative recombination.

A 2D rectangle of the linear size (100×100) as shown in Fig. 3.8 is considered and the periodic boundary conditions are employed. The each site of the rectangle is considered as a localized state. For the Monte Carlo simulation of exciton hopping through the localized states it is assumed that these states are distributed in space at random within the rectangle.

1	2	3	4	.	.	100
2						
3						
4						
.						
.						
100						

- We have
- A region (100×100) with random number of localized states,
 - Unknown amount of energy of each localized states
 - Unknown distances among the localized states
 - Unknown number of excitons that get hop
 - Unknown number of excitons that get recombined

Figure 3.8: Modeling for Monte Carlo simulation of exciton hopping in III-nitride MQWs.

For the each iteration of the simulation process, a particular number of localized states (25%) are considered form the 100×100 number of states as shown in the rectangle of Fig. 3.8. The energies of the selected localized states (sites) were chosen by a random number. The distribution of the energy of each localized states are considered in such a way that a Gaussian DOS is obtained. The energetic parameter of the DOS acts as a scaling parameter for all energies in this simulation technique. Therefore, to perform the Monte Carlo simulation of exciton hopping through the localized states, no correlation between energies of sites and their spatial positions were allowed. Consequently there is no correlation of the distance between the localized states. These sites simulate the set of localized states that an exciton can use for its hopping motion. The rate of a hopping transition from an occupied site i to an empty site j over a distance r_{ij} is determined by the Miller-Abrahams expression [60] as described in previous section

$$v_{ij} = v_0 \exp\left(-\frac{2r_{ij}}{\alpha} - \frac{E_j - E_i + |E_j - E_i|}{2k_B T}\right) \quad (3.7)$$

Hopping and recombination of a large number of excitons n has been simulated independently. The fate of each of them has been studied in the following way. First an exciton is situated at a random site i within the array of sites described above. Then the decay rate v_i is calculated as

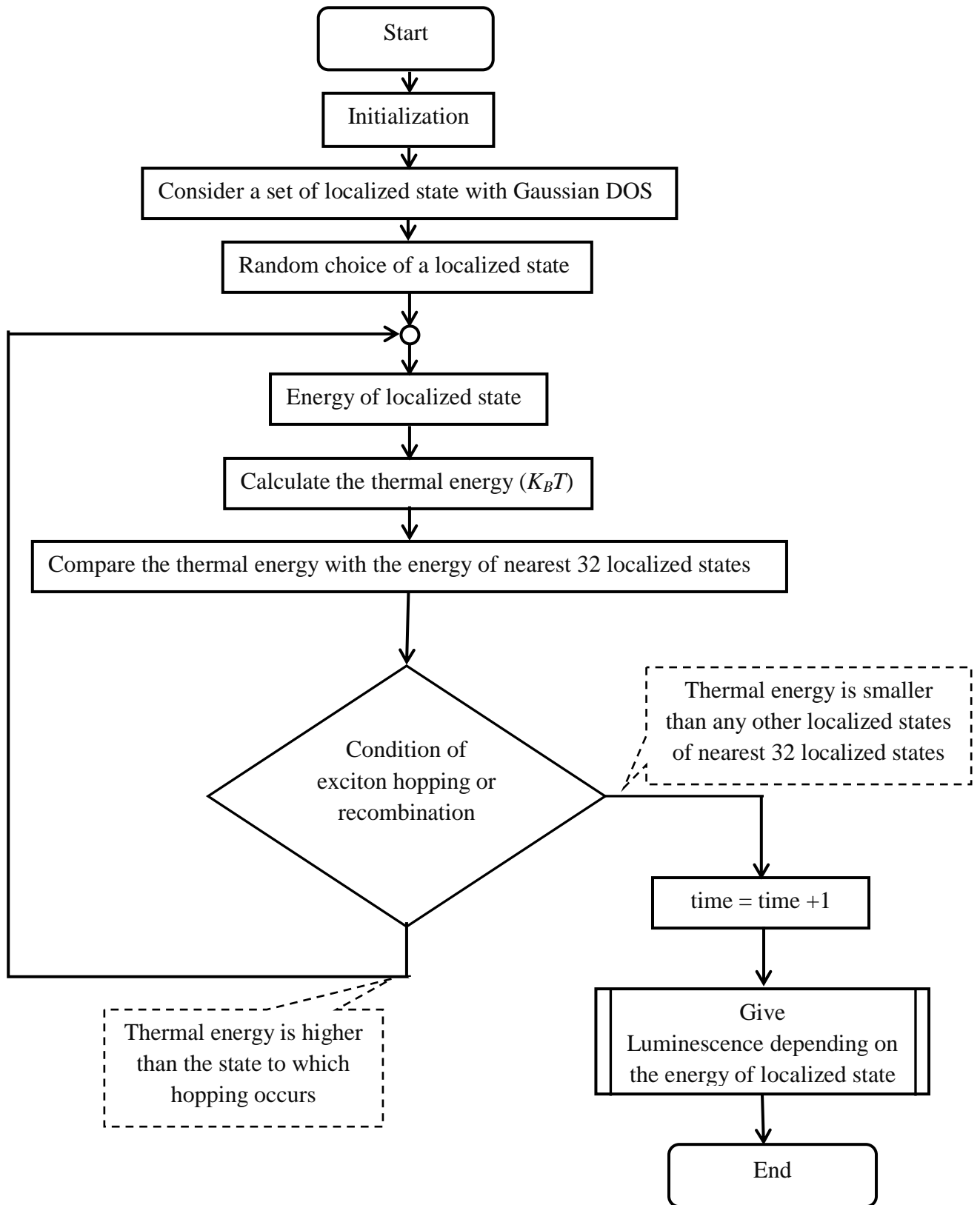


Figure 3.9: Flow diagram to adopt Monte Carlo approach to simulate the exciton hopping and relaxation in III-nitride MQWs.

$$v_i = \tau_0^{-1} + \sum_j v_{ij} \quad (3.8)$$

Because the hopping rates v_{ij} depend exponentially on the distances and energy differences between localized states, only few of them determine the sum in the right hand side of Eqn. (3.8). Therefore, we restricted the number of v_{ij} terms in this sum by M largest terms. Usually M is taken as 32 and it has been checked that the increase of M up to 64 does not change the simulation results [49].

Using a random number generator, the real time t_i of the next process, which is to occur with the chosen exciton, has been calculated as

$$t_i^{-1} = -v \ln \xi_1 \quad (3.9)$$

Where ξ_1 is a random number from the uniform random number distribution between 0 and 1. Then using the rates t_i^{-1} and v_{ij} and another random number ξ_2 the specific process is determined. If it is the hopping transition to some localized state j , the exciton is transferred to the site j , the term t_i is added to the whole time counter, and the algorithm is repeated. If it is the exciton recombination, the energy position of the exciton is stored along with the sum of times t_i , which the exciton has spent for the successive hops, and also for the last step. Then a new exciton is considered, and so on. The results of the simulation are the spectrum of the recombination energies and the distribution of the recombination times for all n excitons. The parameters of the system under consideration, i.e. τ_0 , v_0 , α , and the concentration of the localized states N can be combined into a set of only two essential parameters $N\alpha^2$ and $\tau_0 v_0$. The energies are always scaled by the typical energy scale of the DOS function. The number of sites N_0 was chosen to be equal to 2500 and the number of exciton fates simulated for each set of parameters varied from 10^4 to 10^5 , in order to get the reliable results after the averaging. The flow chart depicted in Fig. 3.9 shows the basic of Monte Carlo simulation to calculate the hopping and relaxation of exciton in MQWs

3.6 Fitting Parameters in Monte Carlo simulation

To make the calculated results for PL peak energy position (First momentum) and line-width (Second momentum) obtained from the Monte Carlo simulation best suited with the experiment, there are two essential fitting parameters. One of them is for the fitting of temporal variation ($N\alpha^2$) and another one is for spatial variation ($\tau_0 v_0$) of experimental results with temperature.

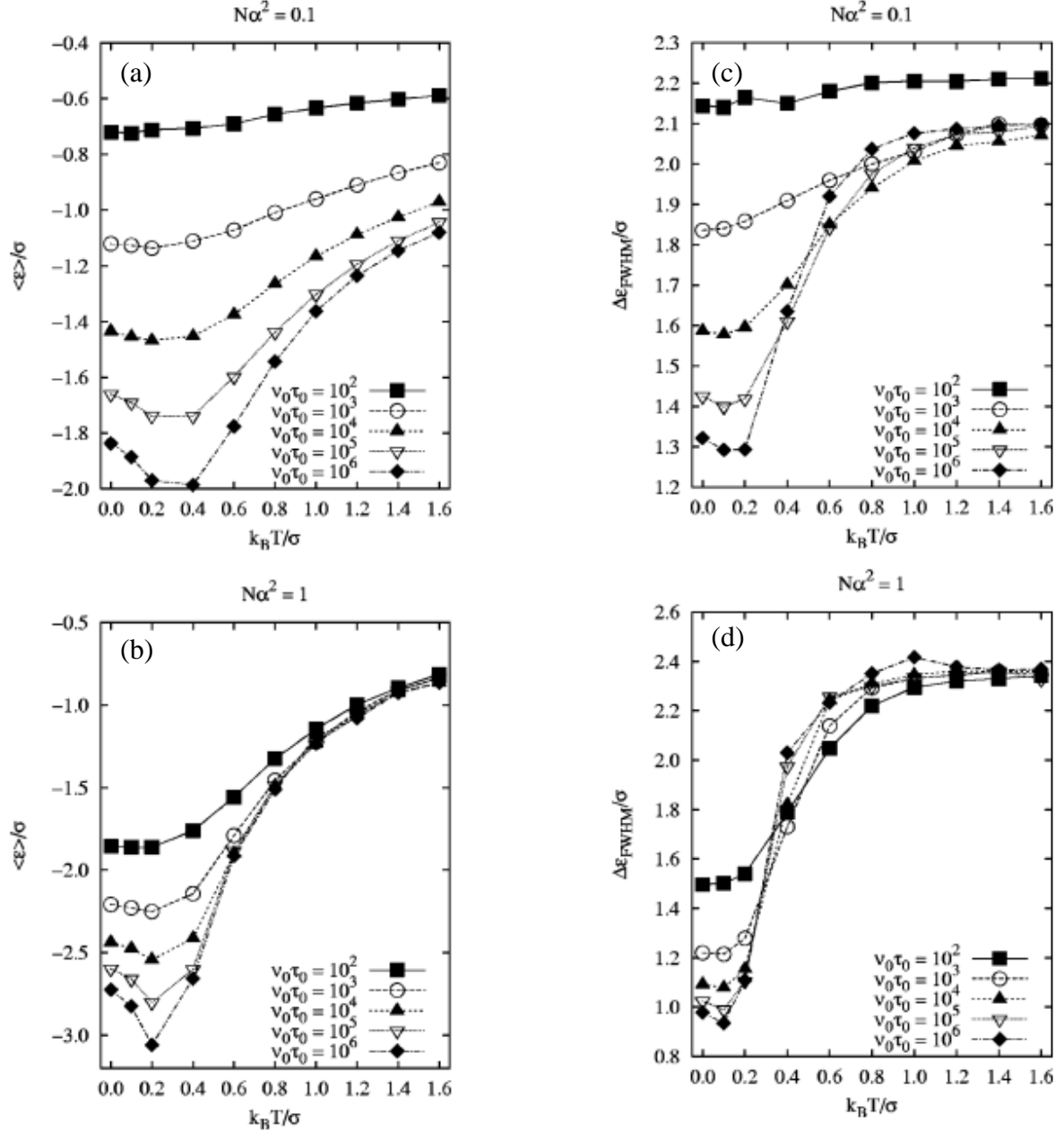


Figure 3.9: The temperature dependence of the PL peak energy position for different values of $\tau_0 v_0$ with (a) $N\alpha^2 = 0.1$ and (b) $N\alpha^2 = 1$, respectively. The temperature induced line-width for different values of $\tau_0 v_0$ with (c) $N\alpha^2 = 0.1$ and (d) $N\alpha^2 = 1$, respectively [49].

3.7.1 Parameter $\tau_0 v_0$

This fitting parameter is used to fit for the spatial variation ($\tau_0 v_0$) of experimental results with temperature. It is found from Fig. 3.9 (a) that for a particular value $N\alpha^2$ with the increase of $\tau_0 v_0$, the value of PL peak energy position shows the greater red shifting behavior with temperature in compare with the smaller $\tau_0 v_0$. It may be due to the reason that the

quantity $\tau_0\nu_0$ is generally increased by increasing the value of τ_0 (the radiative lifetime of exciton). The increased τ_0 allows the carrier to move over deeper localized states. The recombination of exciton from deeper localized states gives the red shifting behavior with temperature. At low temperature, the line-width becomes narrower with increase of τ_0 due to the recombination of exciton from a smaller number of deeper localized states.

3.7.1 Parameter $N\alpha^2$

From the Fig. 3.9 (c) and (d) it is found that for a particular value of spatial variation, $\tau_0\nu_0$ (for example 10^6), the line-width (FWHM) variation with temperature depends on the another fitting parameter $N\alpha^2$. When $N\alpha^2$ is increased, the number of localized states increases. The recombination of exciton from a large number of localized states gives broadened line-width with temperature.

Chapter

IV

RESULTS AND DISCUSSIONS

Chapter at a Glance

- | | |
|--|--------------------|
| • Introduction | Section 4.1 |
| • Photoluminescence study of InGaN/GaN MQWs | Section 4.2 |
| • Photoluminescence study of GaN/AlInN MQWs | Section 4.3 |

4.1 Introduction

In this chapter, the calculated PL spectra have been presented for InGaN/GaN and GaN/AlInN MQWs using the Monte Carlo simulation of phonon-assisted exciton hopping and localization. The simulation results have been shown for the temperature range of 3K to 300K. The peak energy positions and the line-widths of the PL spectra have been calculated for both of MQWs considering the phonon-induced variation of exciton lifetime. The temperature-induced variation of PL peak energy positions and line-widths for InGaN/GaN and GaN/AlInN MQWs has been observed for the entire range of temperature. To investigate the effect of barrier height on the optical properties of GaN/AlInN QW structure, the PL peak energy positions and line-widths have been calculated for GaN/Al_{0.88}In_{0.12}N and GaN/Al_{0.78}In_{0.22}N MQWs.

4.2 Photoluminescence study of InGaN/GaN MQWs

To investigate the temperature behavior of PL spectra in InGaN/GaN MQWs, the Monte Carlo simulation of phonon-induced exciton hopping has been performed considering the structure as shown in Fig. 4.1(a). The structure consists of four-period of In_{0.3}Ga_{0.7}N QWs with the thickness of each 3nm. The QWs are separated by 14nm thick GaN barrier layers deposited on a buffer layer of GaN with the thickness of 2.5μm. Figure 4.1(b) shows the

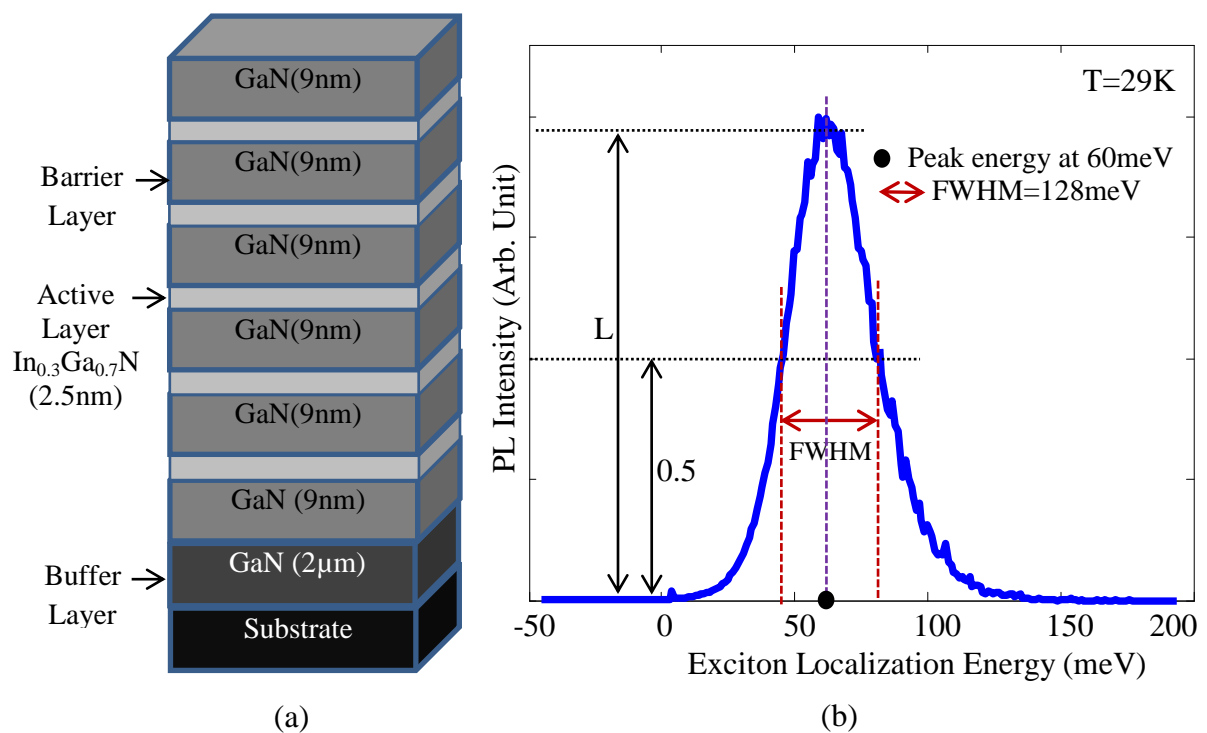


Figure 4.1: (a) Schematic view and (b) calculated photoluminescence spectra with peak energy position and line-width at the temperature of 29K for five-period In_{0.3}Ga_{0.7}N/GaN MQWs

calculated PL spectra from the considering MQWs for a particular temperature of 29K. The line-width or FWHM (full width at half maxima) and the peak energy position of the PL spectra are calculated. It is found that the PL line-width is 128meV. The peak energy position of the PL spectra is found where the exciton localization energy is 60meV. Exciton localization energy is amount of energy by which the energy of emitted photon is smaller than the band-gap energy as shown in Fig. 4.2. The interrelation among the exciton localization energy or exciton energy (E_x), band-gap energy (E) and the energy of emitted photon (E_0) can be estimated

$$E_0 = E - E_x \quad (4.1)$$

The exciton energy can be found from this expression in terms of E_0 and E as follows:

$$E_x = -(E_0 - E) \quad (4.2)$$

Figure 4.3 shows the calculated PL spectra in InGaN/GaN MQW structure for the temperature range of 10K to 300K. The horizontal axis of this figure is in the scale of exciton energy according to the equation of 4.2. The peak positions of the calculated PL bands at various temperatures have been indicated by the dotted line. The PL peak energy positions exhibit the red-shift up to the temperature of 100K and the blue shift is observed till the temperature of 300K.

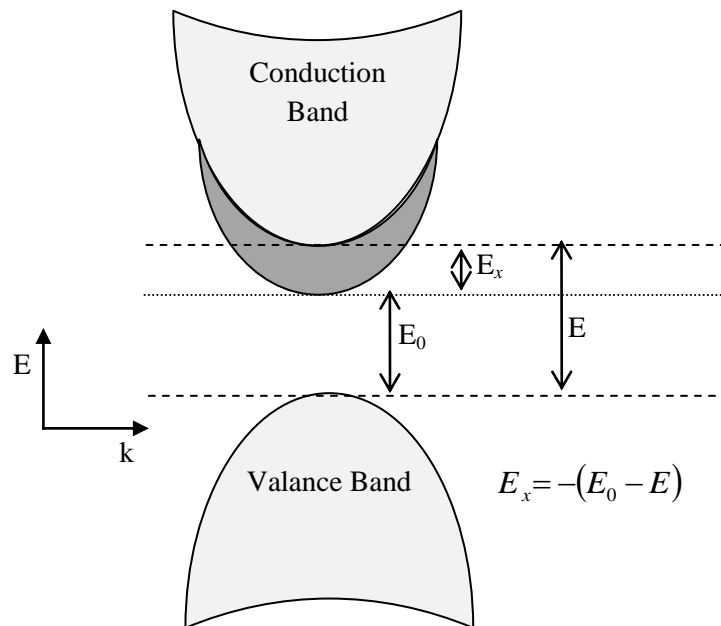


Figure 4.2: Interrelation of Exciton energy (E_x), Band-gap energy (E) and the energy of emitted photon (E_0).

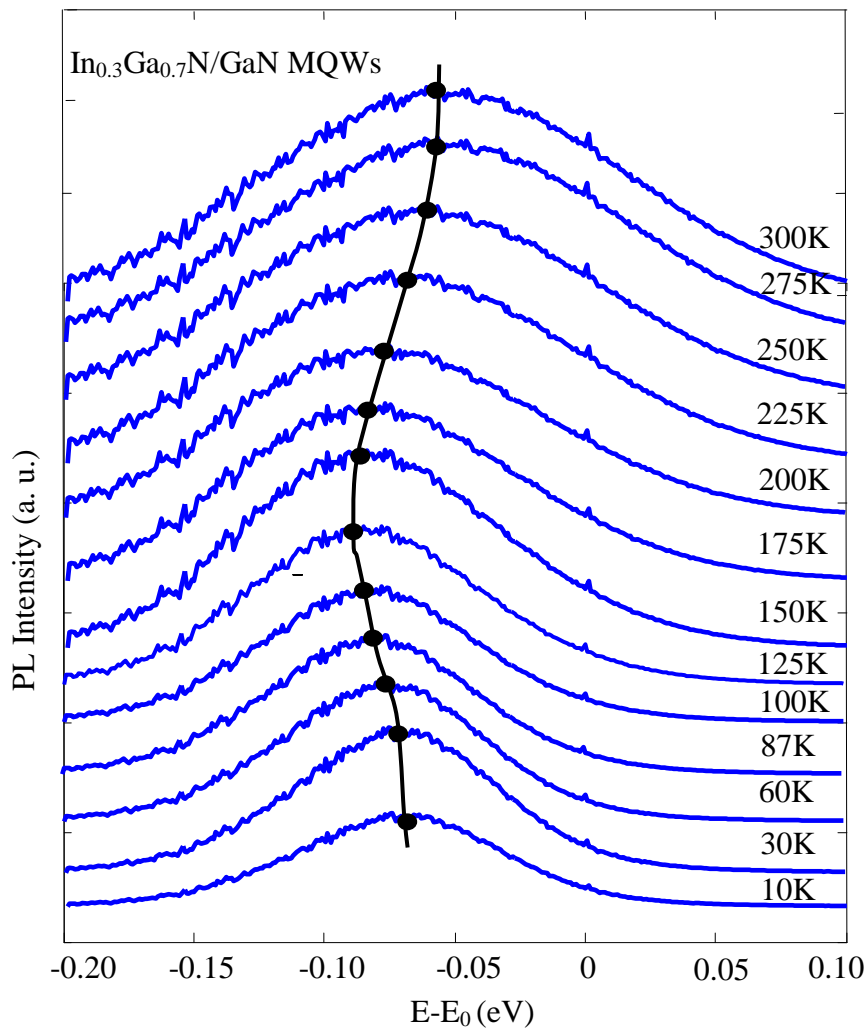


Figure 4.3: Calculated excitonic photoluminescence (PL) spectra of $\text{In}_{0.3}\text{Ga}_{0.7}\text{N}/\text{GaN}$ MQWs for the temperature range of 10-300K. The band peak positions are indicated by the dotted line. The horizontal axis is in units with respect to the exciton energy.

4.2.1 PL Peak Energy Position in InGaN/GaN MQWs

The calculated peak energy positions of the PL spectra in $\text{In}_{0.3}\text{Ga}_{0.7}\text{N}/\text{GaN}$ MQWs with temperature are depicted in Fig. 4.4. The black solid line in Fig 4.4(a) shows the PL peak energy position for conventional Monte Carlo simulation. It is found that the simulation result designates the redshift-blueshift behavior with temperature. Kazlauskas *et. al.* has also shown the similar results [5, 53] for the temperature behavior of PL peak energy positions in $\text{In}_{0.22}\text{Ga}_{0.78}\text{N}/\text{GaN}$ MQWs and $\text{Al}_{0.1}\text{In}_{0.01}\text{Ga}_{0.89}\text{N}$ quaternary alloy using the Monte Carlo simulation of phonon assisted hopping of exciton. However, the experimental works [5, 17, 64-66] reveal the S-shaped (redshift-blueshift-redshift) temperature behavior in contrast with the simulation work (redshift-blueshift). This indicates that the traditional [5, 53] Monte

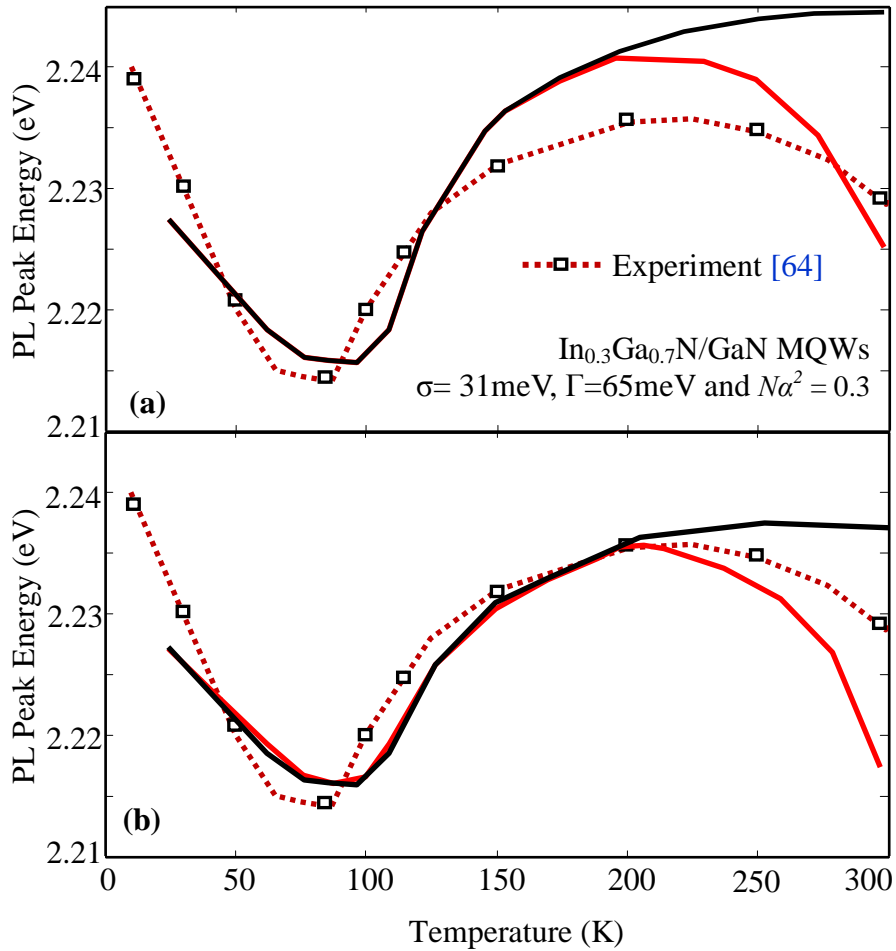


Figure 4.4: The photoluminescence peak energy positions for $\text{In}_{0.3}\text{Ga}_{0.7}\text{N}/\text{GaN}$ MQWs with temperature. The red and the black solid lines show the simulation results considering and without considering the band-gap shrinkage at high temperature, respectively for (a) traditional Monte Carlo simulation and (b) the simulation results with the temperature induced variation of exciton radiative lifetime (τ_0).

Carlo simulation results for the PL peak energy positions are not well matched with the experiment at high temperature.

To achieve the quantitative description of the temperature induced shifting behavior of PL peak energy positions in InGaN/GaN MQWs, the phonon induced variation of exciton radiative lifetime (τ_0) has been integrated in the traditional Monte Carlo simulation of exciton hopping. The earlier studies [5, 22, 53] on the Monte Carlo simulation of exciton hopping reported that the most realistic fitting of the calculated results with experiment depends on the choice of temporal ($N\alpha^2$) and spatial ($\tau_0 v_0$) fitting parameters. These parameters are assigned specified fixed value for the entire temperature range, which implies that τ_0 is also a constant for any temperature. However, the experimental studies [67] indicate that the change in

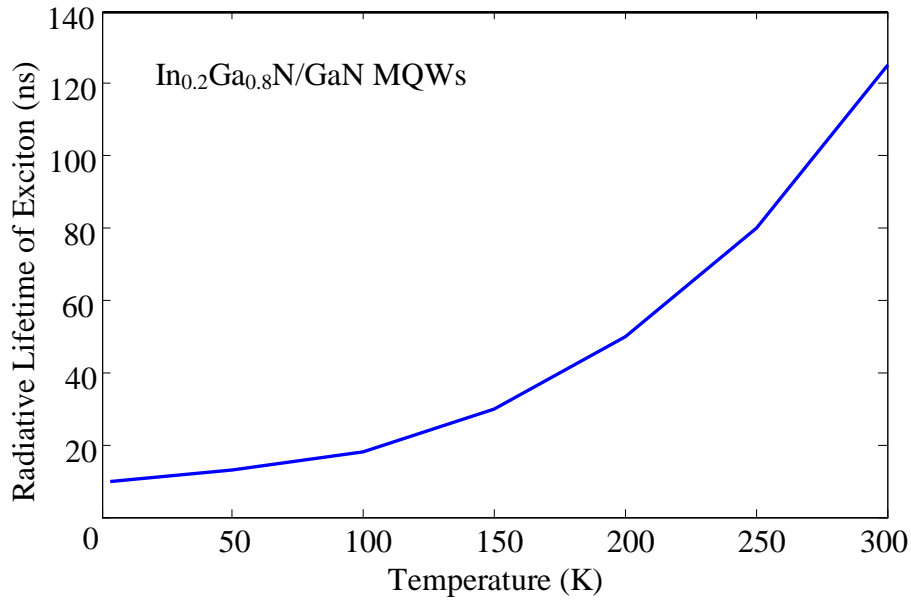


Figure 4.5: Temperature dependent radiative lifetime of exciton in $\text{In}_{0.2}\text{Ga}_{0.8}\text{N}/\text{GaN}$ MQWs. The thicknesses of well and barrier layer are 3nm and 4.3nm, respectively [67].

temperature affects the τ_0 in Indium containing ternary alloys i.e. $\tau_0\nu_0$ is affected by phonon particle. The phonon-induced variation of radiative lifetime of exciton [67] has been shown in the inset of Fig. 4.5. At high temperature, the sharp direct recombination of exciton cannot be resolved due to the thermal activation of non-radiative centers such as dislocation and other defects [68]. Additionally, the excitons are supposed to thermal activation form strongly localized states caused by the coupling with phonon particle at high temperature. There occurs the thermal redistribution of exciton over the localized states. The degree of interaction between the phonon and excitons increases which indicates the thermally activated increase of lifetime in addition to vibration. The temperature-induced increased lifetime gives chance the excitons to hop deeper localized states. Considering the phonon-induced variation of the radiative lifetime of exciton, the PL peak energy position has been depicted in Fig. 4.4(b) by the solid black line. However, a small deviation of simulation results is still visible from the experiment at high temperature.

To minimize the gap between the simulation results and experiment at high temperature, the temperature dependent band-gap shrinkage [69, 70] has been included in the simulation to calculate the PL peak energy position. The temperature-induced fundamental band-gap shrinkage of InGaN is given by the Varshni empirical equation.

$$E(T) = E_g(0) - \frac{\alpha T^2}{T + \beta} \quad (4.3)$$

The term, $E_g(0)$ is the transition energy at 0K and α and β are the Varshni thermal coefficient [71]. Using the values of Varshni thermal coefficient for the Indium composition of 30% in InGaN layer, the amount of band-gap shrinkage is 20mev for the temperature of 200K to 300K. By including the band-gap shrinkage to the calculation of PL peak energy position, the simulation results show the good quantitative fit with the experiment. In Fig. 4.4(a) the red solid line indicates the PL peak energy considering only the band-gap shrinkage with temperature. In Fig. 4.4(b), the red solid line shows the PL peak energy position considering both the temperature induced variation of radiative lifetime of exciton and band-gap shrinkage. Therefore, the PL peak energy positions are well-agreed with experiment while considering the temperature induced variation of exciton radiative lifetime as well as band-gap shrinkage. Thus the following description gives the possible explanation of temperature induced localization dynamics of exciton in InGaN/GaN MQWs for the entire temperature regime of 10K to 300K.

At very low temperature ($\sim 10\text{K}$), the excitons are randomly trapped in the potential minima. The recombination of the trapped excitons produces the luminescence corresponding to the energy of potential minima (localized states). In contrary to the recombination of single electron and hole via tunneling processes, excitons have some typical lifetime with respect to their radiative recombination [72]. However, till the temperatures of 100K, only the weakly localized excitons are activated by the phonon particle. The activated excitons get relaxed down to their neighboring strongly localized states. Thus, an initial red-shift is visible for the peak energy position of the PL spectra from the redistributed excitons. At medium temperature range (100-200K), the phonon particle enables exciton to achieve the thermal equilibrium with the lattice and occupy the localized states with comparatively higher energy. The recombination of localized exciton at higher energy states results in the blue-shift of the PL peak energy. Finally, at high temperature (200K-300K), the peak energy decreases due to the phonon induced broadening of exciton radiative lifetime and typical band-gap shrinkage with temperature.

4.2.2 PL Line-Width in InGaN/GaN MQWs

Figure 4.6 shows the temperature behavior of the calculated full width at half maxima (FWHM) of PL bands displayed in Fig. 4.3. At first, the PL FWHM has been calculated considering the band potential fluctuation within the Indium-rich regions [53] in the ternary alloy. Especially, in InGaN/GaN MQWs, these regions originate due to the limited solubility

of Indium into the GaN matrix. However, the W-shaped behavior of PL FWHM is attributed to the phonon-induced recombination mechanism of exciton. At low temperature (<100K), the excitons are unable to attain the equilibrium distribution within the localized states due to their finite lifetime. Thus, the recombination of excitons leads to the narrower line-width. At medium temperature range (100-200K), an abrupt increase of line-width is visible due to the transferring of excitons from non-thermalized to thermalized distribution over the localized states. At high temperature, the line-width is obtained due to the coupling of exciton to the acoustic phonons as well as longitudinal-optical phonons [64]. Nevertheless, to find the most realistic fitting of the simulation results with the experiment, the dispersion of the distribution of localized states (DOS), σ within the Indium-rich regions is chosen from the approximation $\sigma = 2K_B T_{kink}$, where K_B is the Boltzmann's constant and the value of T_{kink} is chosen from experimental [5, 53] line-width of the PL bands. For this simulation, the value of T_{kink} is chosen 150K, which gives dispersion parameter, $\sigma=31\text{meV}$. Using this dispersion parameter, the simulated FWHM (black solid line) appears to be much narrower than the experiment (solid line indicating right side scale). To achieve a quantitative description of the PL FWHM, additional inhomogeneity parameter Γ (meV) is incorporated to the Gaussian DOS to indicate the band potential fluctuation among the regions i.e. the average localization energy of the individual Indium-rich regions [53]. Thus, the actual density of localized states with energy becomes:

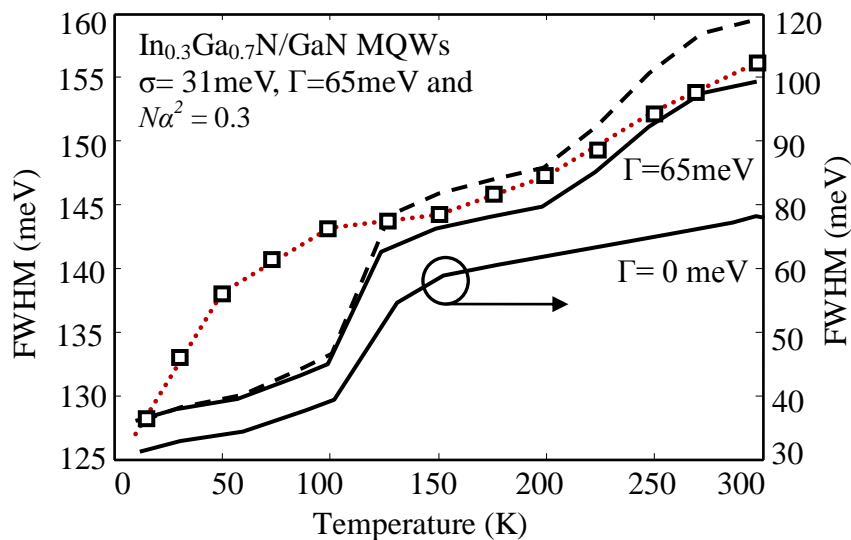


Figure 4.6: The PL FWHM of photoluminescence bands for $\text{In}_{0.3}\text{Ga}_{0.7}\text{N}/\text{GaN}$ MQWs with temperature. The dotted line shows the experimental [64] FWHM. The solid lines show the simulated FWHMs, for $\Gamma=0\text{meV}$ and $\Gamma=65\text{meV}$ respectively. The dashed line indicates the simulated FWHM considering $\Gamma=65\text{meV}$ and phonon induced radiative lifetime of exciton.

$$D(E) \propto \exp\left[-\frac{(E - E_0)^2}{2(\sigma^2 + \Gamma^2)}\right] \quad (4.4)$$

The inhomogeneity parameter, Γ strongly depends on the Indium composition of the active/barrier layer of MQWs. When Indium composition is of 30% in the active layer of InGaN/GaN MQW, the value of Γ is approximated [5] as 65meV. The upper solid line in Fig. 4.6 show the calculated line-width using the Monte Carlo simulation technique while $\sigma=31$ meV and $\Gamma=65$ meV. The dashed line shows the PL FWHM considering the temperature-induced variation of exciton lifetime with additional inhomogeneous broadening. From Fig. 4.6, it is found that our simulation results quantitatively agree with the experimental PL line-width over a wide range of temperature.

From Fig. 4.4 and Fig. 4.6, a good quantitative agreement between the simulation results and experiment is obvious for PL peak energy position and line-width over a wide range of temperature for MQW structure of InGaN/GaN. However, the precision of our simulation results with experiment implies that the temperature behavior of the emission spectra in In_{0.3}Ga_{0.7}N/GaN MQW can be estimated by the Monte Carlo simulation of phonon-assisted exciton hopping and relaxation. We suggest that this approach could be successfully applied to describe the temperature dependent emission spectra in other III-nitride semiconductor based MQW structures as well. In the following section, the temperature-induced behavior of PL peak energy and the line-width have been quantitatively described by the same simulation technique.

4.3 Photoluminescence study of GaN/AlInN MQWs

The temperature dependent optical behaviors of GaN/AlInN MQWs structure have been investigated using the Monte Carlo simulation of phonon-assisted exciton hopping and relaxation. Exciton hopping is simulated for thirty-period of GaN QWs with the thickness of each 1.5nm as clearly shown in Fig. 4.7. The QWs are separated by 3.4nm thick Al_{0.88}In_{0.12}N barrier layer which is deposited on 2 μ m template layer. The simulation is performed considering the potential profile fluctuation, σ and the additional inhomogeneous broadening, Γ . The fitting parameter for spatial variation, $N\alpha^2$ is chosen according to InGaN/GaN MQWs. The Monte Carlo simulation is performed considering the temperature dependent variation of exciton lifetime as discussed before for InGaN/GaN MQW structure i.e. the fitting parameter, $\tau_0\nu_0$ for temporal variation changes with temperature.

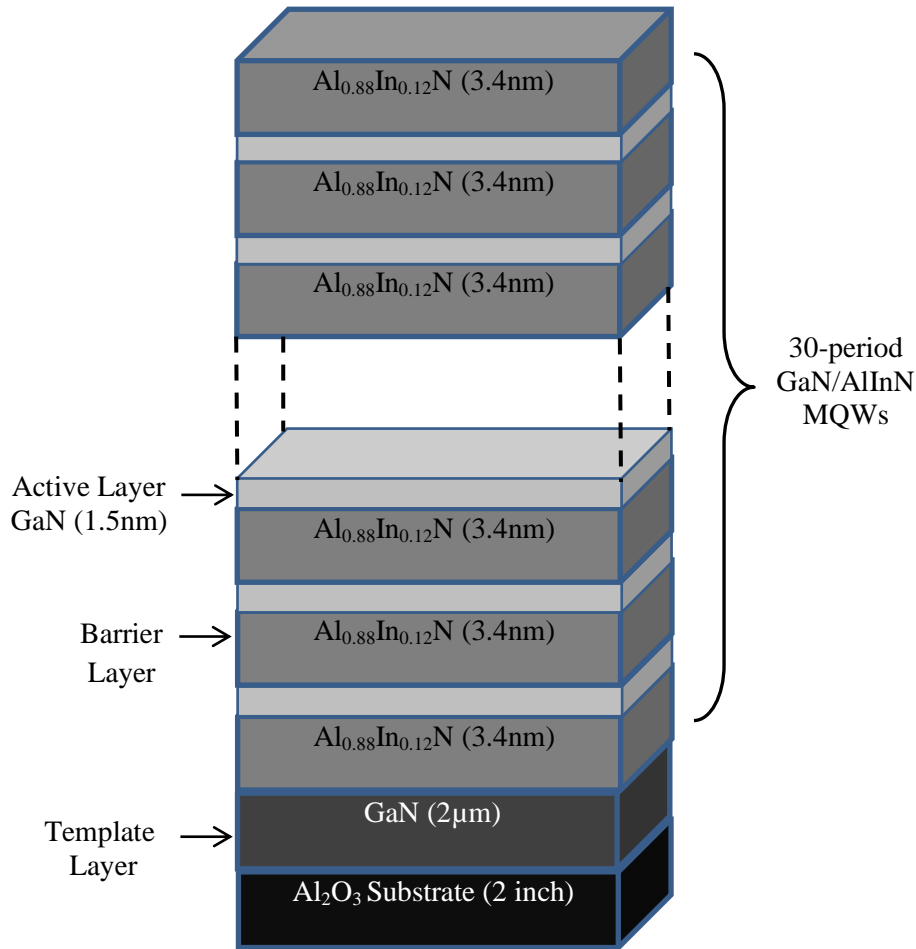


Figure 4.7: Schematic view of thirty period GaN/ $\text{Al}_{0.88}\text{Ga}_{0.12}\text{N}$ MQWs. The thicknesses of well and barrier layer are 1.5nm and 3.4nm, respectively.

Figure 4.8 shows the calculated excitonic PL spectra for thirty-period of GaN/ $\text{Al}_{0.88}\text{Ga}_{0.12}\text{N}$ MQWs for the temperature range of 3K to 300K. The horizontal axis is in the scale of exciton localization energy or exciton energy according to the equation (4.2). The PL peak energy positions have been highlighted by the dashed line. It is found that the PL peak energy positions exhibits the red-shift up to the temperature of 100K then the blue-shift is observed till the temperature of 300K. In InGaN/GaN MQWs, the red-shifting behavior is visible up to the temperature of 87K which is lower than GaN/AlInN MQWs. This phenomenon indicates that the excitons are strongly localized in GaN/AlInN MQWs than the InGaN/GaN MQWs. The line-widths and peak energy position of each PL bands obtained from GaN/AlInN MQWs have been calculated. The temperature dependent behaviors of PL line-width and peak energy in the above MQWs have been discussed in the following sections.

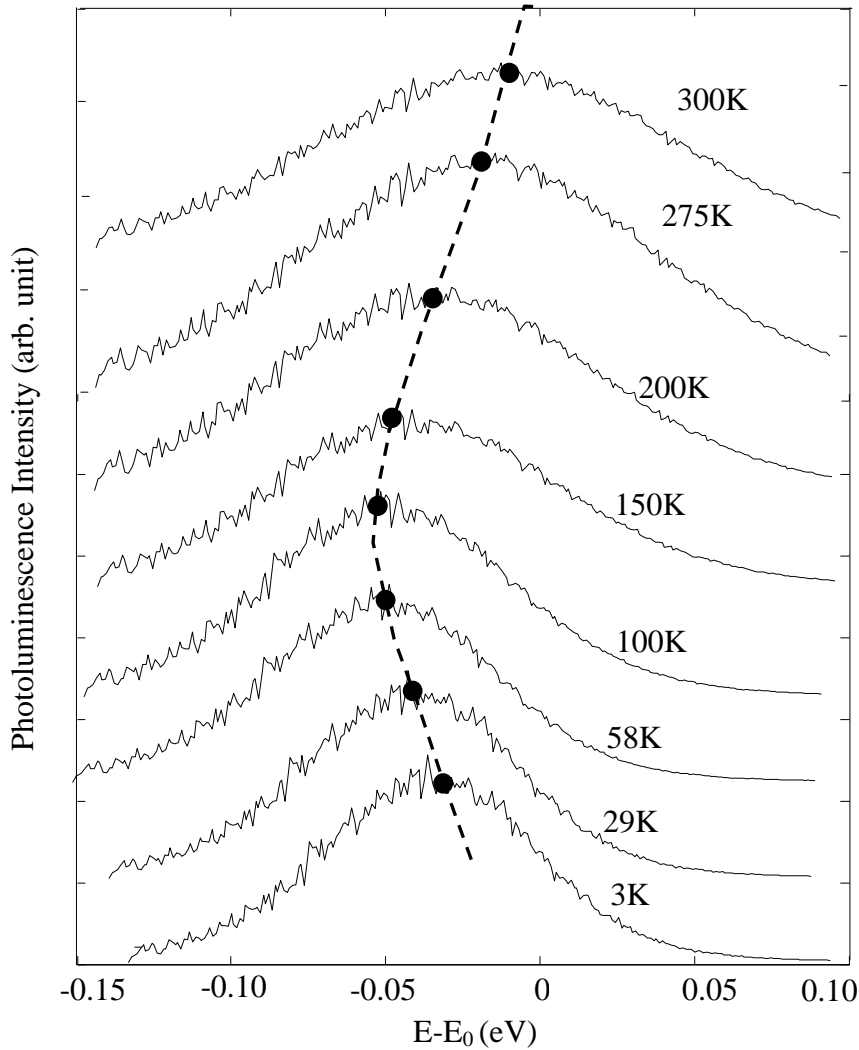


Figure 4.8: Calculated excitonic photoluminescence (PL) spectra of GaN/Al_{0.88}In_{0.12}N MQWs for the temperature range of 3-300K. The band peak positions are indicated by the dashed line. The horizontal axis is in units with respect to the exciton energy.

4.3.1 PL peak energy in GaN/AlInN MQWs

The dashed line in Fig. 4.9 (a) shows the simulated PL peak energy position for GaN/Al_{0.88}In_{0.12}N MQWs structure for the temperature range of 3K to 300K. The calculated PL peak energy positions exhibit the S-shaped shifting behavior with temperature. It is found that the simulation results are well-matched with the experimental values [7] for the entire range of temperature from 3K to 300K. In Fig. 4.10 (a), the line-width of the calculated PL bands from GaN/Al_{0.88}In_{0.12}N MQWs are also well-agreed with the experiment [7] which will be analyzed later. The matching of simulation results with the experiment supports the pronounced effect of hopping and relaxation of localized exciton in fluctuated band structure of GaN/AlInN MQWs.

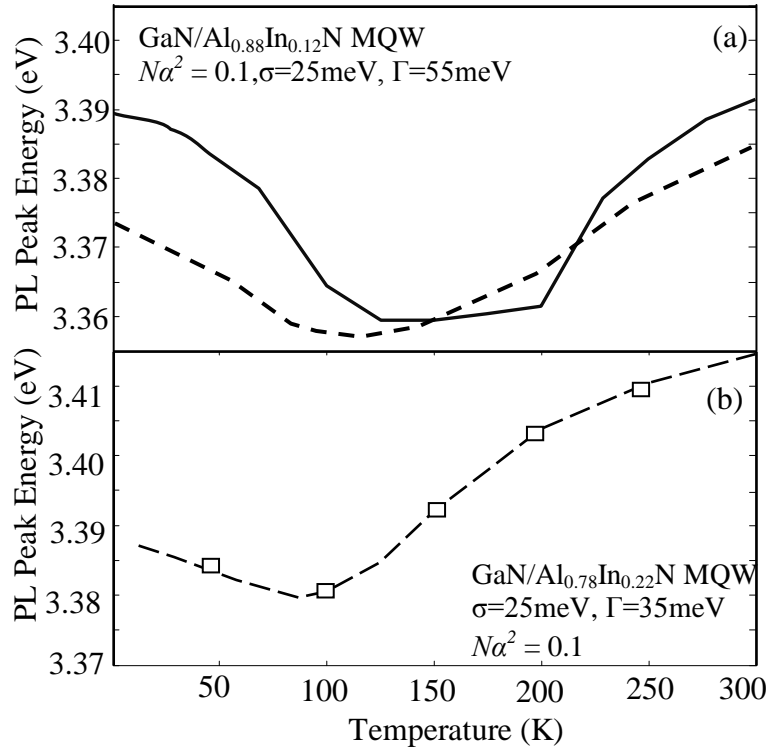


Figure 4.9: (a) The peak energy positions of the PL bands for GaN/Al_{0.88}In_{0.12}N MQWs with temperature. The solid line shows the experimental [7] PL peak energies whereas the dashed line indicates the simulation results. (b) Temperature dependent PL peak energy position of GaN/Al_{0.78}In_{0.22}N MQW.

It has also been examined, for comparison, the temperature dependence of PL peak energy positions in a MQWs having lower barrier height: a GaN/Al_{0.78}In_{0.22}N MQWs with remaining identical features of GaN/Al_{0.88}In_{0.12}N MQWs. In Fig 4(b), the PL peak energy positions in GaN/Al_{0.78}In_{0.22}N MQWs show the reduced S-shaped behavior with temperature. This may be due to the degree of localization i.e. the potential profile fluctuation in Al_{1-x}In_xN barrier layers [8].

4.3.2 PL line-width in GaN/AlInN MQWs

At first, the line-width of GaN/Al_{0.88}In_{0.12}N MQWs have been calculated using $\sigma = 25\text{meV}$, $\Gamma = 55\text{meV}$ and $N\alpha^2 = 0.1$. The temperature induced lifetime variation has been considered as discussed before. The dashed line in Fig. 4.10(a) shows the calculated PL FWHM in GaN/Al_{0.88}In_{0.12}N MQWs for the temperature range of 3K to 300K. It is found that with the change of temperature from 3k to 300K the PL FWHM changes from 90meV to 150meV. Additionally the PL FWHM has been calculated for GaN/Al_{0.78}In_{0.22}N MQWs. The indium composition in GaN/Al_{0.78}In_{0.22}N MQWs is more nearer to the lattice matched structure [8] ($x \sim 19\%$) of GaN/AlInN QWs than GaN/Al_{0.88}In_{0.12}N MQWs. The more difference with

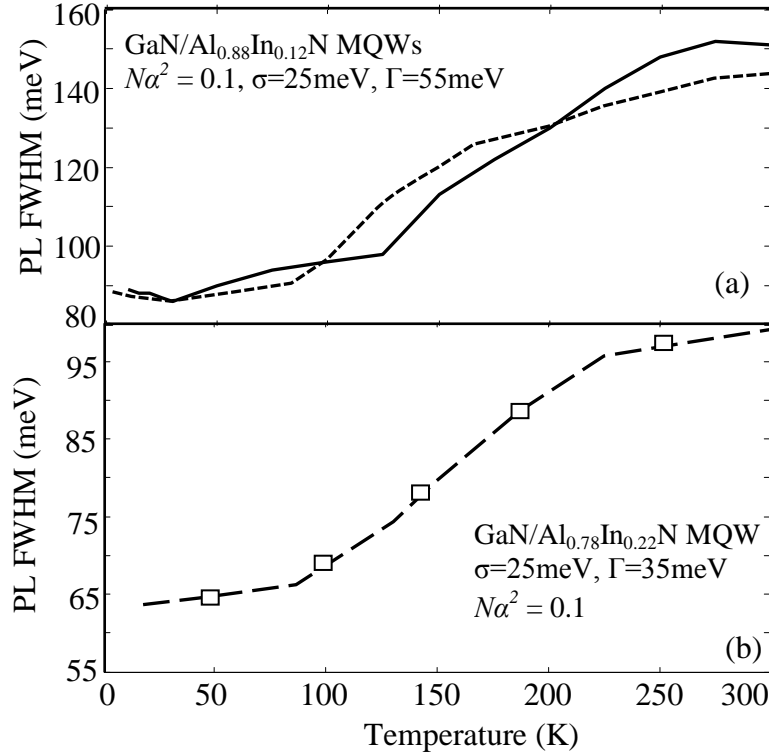


Figure 4.10: (a) The FWHM for GaN/Al_{0.88}In_{0.12}N MQW with temperature. The solid line shows the experimental [7] PL FWHM whereas the dashed line indicates the simulation results. (b) Temperature dependence of FWHM of GaN/Al_{0.78}In_{0.22}N MQWs.

lattice matched composition causes more band potential profile fluctuation in AlInN alloy which results in broaden DOS for localized states in GaN/AlInN MQWs. Therefore, it can be approximated that the line-widths of the PL bands for the GaN/Al_{0.78}In_{0.22}N MQWs could be smaller than the line-widths from GaN/Al_{0.88}In_{0.12}N MQWs. The PL FWHM for GaN/Al_{0.78}In_{0.22}N MQWs are calculated for smaller value of Γ compared to the GaN/Al_{0.88}In_{0.12}N MQWs. It is found that with the change of temperature from 3k to 300K the PL FWHM changes from 65meV to 100meV. It is found that the two MQWs, having different barrier heights exhibited unlike PL line-width with temperature.

Chapter

V

SUMMARY AND OUTLOOK

Chapter at a Glance

- **Conclusion**
- **Future Work**

Section 5.1

Section 5.2

5.1 Conclusion

This dissertation focused on the details of inhomogeneous localization dynamics of exciton in InGaN/GaN and GaN/AlInN MQWs for a wide range of temperature. A quantitative model has been developed based on the modified Monte Carlo simulation of exciton hopping. This model qualitatively describes the temperature-induced inhomogeneous behavior of PL peak energy positions and line-widths in both MQW structures. The results obtained by the developed model have been compared with the experimental results and found to be very good agreement.

An S-shaped (redshift-blueshift-redshift) temperature dependence has been observed for the peak energy positions of PL spectra in InGaN/GaN and GaN/AlInN MQWs. Additionally, the W-shaped behavior of the line-widths of PL bands is apparent with temperature for both MQWs. The simulation results exhibit a good quantitative fit with the experimental unusual feature of PL maximum and line-width with temperature while considering the temperature-induced variation of exciton lifetime in conventional Monte Carlo simulation of phonon-assisted exciton hopping and relaxation. The matching of simulation results with experiment reveals that 2D excitonic kinetics is dominant for the entire range of temperature for the MQWs having well and barrier thicknesses near about their critical values. For such type of MQWs, the possibility of the origination of dislocation or other nonradiative recombination centers is low due to the lower thickness of well and barrier layer. The minor existence of non-radiative centers indicates the more enhancement of the non-radiative recombination lifetime than radiative lifetime which indicates the dominancy of radiative lifetime in PL decay time. At low temperature, the excitons get recombined maintaining their lifetime. With the increase of temperature, the interaction between phonon and exciton increases which leads to the broadening of exciton lifetime. The enhanced lifetime of exciton decreases the recombination energy as consumption of energy due to vibration increases.

The effect of barrier height on the inhomogeneous optical behavior is also investigated for GaN/AlInN MQWs. Significantly different temperature dependences for PL line-widths are observed for the GaN/AlInN MQWs with different barrier heights. The MQWs having barrier height near to the lattice matched quantum well structure of GaN/AlInN show smaller variation of W-shaped PL line-width which indicates the smaller band potential profile fluctuation. The well-matching of the calculated results with experimental S-shaped PL maximum and W-shaped line-width indicates the formation of potential roughness due to inhomogeneous Indium distribution in ternary alloys.

These results could be important to understand the realistic optical properties for the advancement of InGaN and AlInN MQW based optoelectronic devices.

5.2 Future work

The modified Monte Carlo simulation technique described in this dissertation has proven to accurately describe the inhomogeneous PL behavior of InGaN/GaN and GaN/AlInN MQWs for a wide range of temperature. At the same time, there have been several important physical issues to the origination of light emission from III-nitride QW structure that remain to be incorporated in the simulation technique. These include the determination of actual density of localized states (DOS) with the energy, the effect of phonon DOS.

The Monte Carlo simulation technique in this thesis has been performed in 2D manner. The modified Monte Carlo method can be extended to the three dimensions (3D) to calculate the PL spectra in III-nitride MQWs. For calculating the hopping of excitons from one state to another, the Millar-Abrahams's rate has been considered. In Miller-Abraham's rate of phonon-assisted hopping process, the dependence of hopping rates on distance and the dependence of the mobility on temperature are assumed similar which is not the actual case.

Appendix

Appendix A: Monte Carlo technique to calculate ‘pi’

A Monte Carlo method [62] is a mathematical model that relies on chance or repeated random behavior in order to determine a solution to a problem. In the following section, the Monte Carlo technique has been used to determine the value of ‘pi’. Consider a circle inscribed within a square, like a dart board, as shown Fig. 3.7. Notice that the width of the circle is equal to the width of the square. The square has length and width equal to the diameter of the circle or twice the radius, i.e. $2r$, where r is the radius of the circle. Now, considering the Fig. 3.7, the area of the circle and surrounding square can be given as:

$$A_c = \pi \times r^2 \quad (3.5)$$

$$A_s = l \times w = d \times d = d^2 = (2r)^2 = 4r^2 \quad (3.6)$$

If we compare the area of the circle with the area of the square, we can form a ratio as follows:

$$\frac{A_c}{A_s} = \frac{\pi \times r^2}{4r^2} = \frac{\pi}{4} \Rightarrow \pi = 4 \frac{A_c}{A_s} \quad (3.7)$$

In other words, ‘pi’ is equal to the ratio of the area of an inscribed circle to the area of outer square multiplied by 4.

It is imagined that we are able to throw darts (or marbles) at random locations on our considered region as shown in Fig. 3.7. With the increase in time, the percentage of random darts striking the circle will be proportional to the area of the circle as a percentage of the total square area. In other words, if we throw ten darts and seven of them land in the circle then the area of our circle is roughly 7/10 or 70% of the area available. If we throw twenty

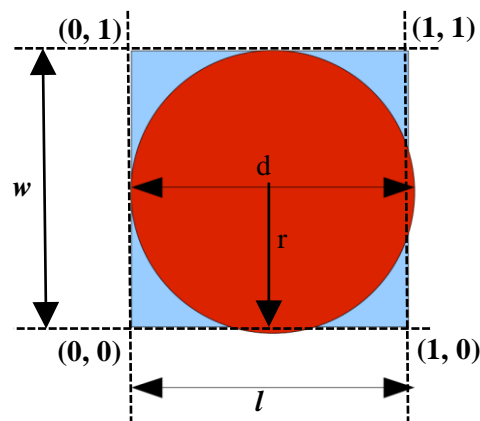


Figure A.1: Monte Carlo simulation approach to estimate the value of ‘pi’.

darts and twelve darts land within the circle, then we would estimate the area of the circle to be 12/20 or 60% of the total area. Using this idea of darts, then, we can determine through chance (Monte Carlo simulation) a rough value for the ratio of the area of the circle to the total area:

$$\frac{A_c}{A_s} = \frac{\text{number of darts landing inside the circle}}{\text{total number of darts thrown}} = \text{hit \%}$$

and from this ratio, a value for ‘pi’:

$$\pi = 4 \frac{A_c}{A_s} = 4 \times \text{hit \%} \quad (3.8)$$

MATLAB or FORTRAN (or equivalent) is used to generate the random numbers that will represent each dart's “position” on the region and to calculate whether each dart represents a “hit” or falls outside the circle.

- ✓ first random number will be assigned as the x -coordinate of our first dart
- ✓ second random will be assigned as the y -coordinate of our first dart
- ✓ third random number will be assigned as the x -coordinate of our second dart
- ✓ fourth random number will be assigned as the y -coordinate of our second dart
- ✓ next random number ... x -coordinate of third dart
- ✓ next random number ... y -coordinate of third dart
- ✓ continuing this pattern for each “dart” we care to throw (start with around 100 or other number of “darts”)

Imagine that a unit circle is centered in a unit square. Imagine the square on the (x, y) origin such that the lower left corner of the square coincides with point $(0, 0)$ as shown in Fig. 3.7. The square, then, runs up to point $(0, 1)$ and across to points $(1, 0)$ and $(1, 1)$. The center of the square, as well as the center of its inscribed circle, lies at point $(0.5, 0.5)$.

Each set of two random numbers represents the random co-ordinate of each dart. For each set, the distance from the center point $(0.5, 0.5)$ is calculated and compared with the calculated radius of the circle. The distance can be calculated by geometrical equation as follows:

$$d = \sqrt{(x_2 - x_1)^2 + (y_2 - y_1)^2} \quad (3.9)$$

Appendix B: Derivation of DOS:

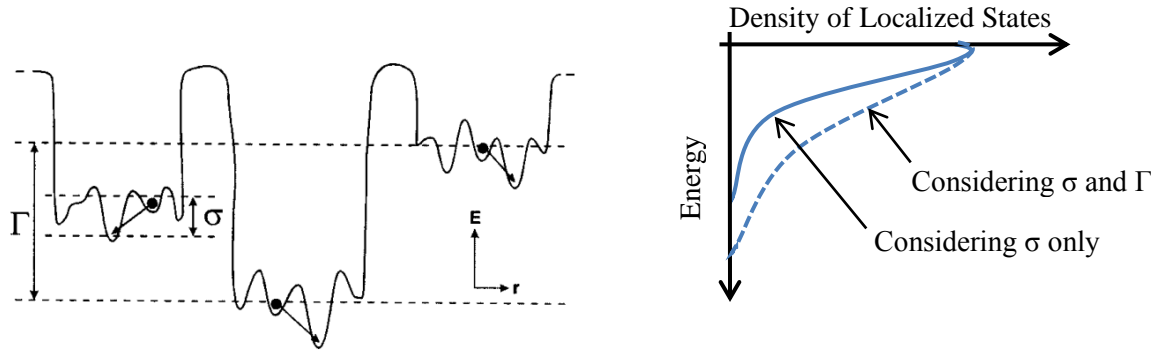


Figure 3.4: (a) Schematic plot of a disorder induced potential profile in InGaN alloy and (b) Gaussian DOS showing dispersion of the distribution of localized states within the cluster, σ and among the clusters, Γ [53].

The derivation of the density of localized state considering σ and Γ :

Considering only σ , the DOS is given by

$$D_1(E) \propto \exp\left[-\frac{(E - E_0)^2}{2\sigma^2}\right]$$

$$\ln D_1(E) \propto \frac{2\sigma^2}{(E - E_0)^2}$$

Again considering only Γ , the DOS is given by

$$D_2(E) \propto \exp\left[-\frac{(E - E_0)^2}{2\Gamma^2}\right]$$

$$\ln D_2(E) \propto \frac{2\Gamma^2}{(E - E_0)^2}$$

Now the actual density of state considering σ and Γ can be written

$$\begin{aligned} \ln D(E) &\propto \ln D_1(E) + \ln D_2(E) \\ &\propto \frac{2\sigma^2}{(E - E_0)^2} + \frac{2\Gamma^2}{(E - E_0)^2} \\ &\propto \frac{2(\sigma^2 + \Gamma^2)}{(E - E_0)^2} \end{aligned}$$

$$\ln D(E) \propto \exp \frac{2(\sigma^2 + \Gamma^2)}{(E - E_0)^2}$$

$$D(E) \propto \exp \left[-\frac{(E - E_0)^2}{2(\sigma^2 + \Gamma^2)} \right]$$

Appendix c: MATLAB Code for Monte Carlo simulation of Exciton Hopping

```
clc;
clear;
tic;

mx=100;
my=100;
idim=mx*my; % simulation area
mcut=32; % M largest terms 32~64 probability of changing of hoping rate
nhiste=150; % 0~150 localized states in eV depends on material and
composition
nhistt=10;
maxiter=100000;
maxilcl=100;

temp=input('input the temperature:'); %

% c input data

sigma=28; % for InGaN 31meV when Indium composition 22%
e0=0;
acut_1=0; % for InGaN 0meV for gauss distribution%
acut_2=-150; % for InGaN 190meV for gauss distribution when Indium
composition 22%%

arate=0.25; % N in gauss distribution%
anu0=2e12; % attempt to escape frerquency (energy)
tau0 = 1e-10; % exciton lifetime
alpha2_n=1; % decay length of exciton
ehist = -acut_2;
thist=1e-3;
adt = thist/nhistt;
ade = (ehist + acut_1)/nhiste;

% initialization %%call init(idim,nhiste,nhistt,time,histe,histt)

time=zeros(idim);
histe=zeros(nhiste);
histt=zeros(nhistt);
% % for i = 1:idim
% % time(i) = 0;
% % end
% %time=zeros(idim);
% for i = 1:nhiste
% histe(i) = 0;
% end
%
% for i = 1 : nhistt
% histt(i) = 0;
% end

inorm = 0;
maxmonte=100;
```

```

isx=zeros(idim);
isy=zeros(idim);
isp=zeros(mx,my);

for ilcl = 1: maxilcl

    % step 1#: random choice of site %%%%%%%%%%

    % site selection site(mx,my,idim,isx,isy,kseed1,nmax,arate)

    %sgrnd = rand(1);
    for i = 1:idim
        isx(i) = 0;
        isy(i) = 0;
    end

    nn = 0;
    for i = 1:mx
        for j = 1:my

            isp(i,j) = 0;

        end
    end

    r= rand(1);
    if(r<=arate)
        nn = nn + 1;
        isx(nn) = i;
        isy(nn) = j ;
        isp(i,j)=nn;
    end
end

nmax = nn % number of localized states in each iteration

% site =rand(100,100);
% c step 2-1: distribution of energy

anu=0.5/(sigma^2);
ad0=(arate^2)/(2*pi*(sigma^2));
ad0=sqrt(ad0);

% Calculation of energy distribution
endis(mx,my,idim,en_dis,anu,ad0,e0,& acut_1,acut_2,kseed2,nmax)

%en_dis(idim);
numb = 3000; % energy deference point in gaussian distribution
add = (acut_1 - acut_2)/numb;
anorm=0;
for i = 1:numb
    eng = acut_2 + i*add;
    anorm = anorm + ad0*exp(- anu*((eng-e0)^2) )*add ;
end

for i = 1:nmax
    r1= rand(1);

```

```

aSUM = 0;
bSUM = 0;
en_dis(i) = 0;
for inum = 1: numb+1
    eng = acut_2 + inum*add ;
        bSUM = aSUM + ad0*exp(-anu*((eng-e0)^2) )*add/anorm
;
        if(r1>=aSUM && r1<bSUM)
            en_dis(i) = eng;
        end
        aSUM = bSUM;
end
end

for i = nmax+1: idim
    en_dis(i) = 10000;
end

    en1 = 0;
for i = 1:nmax
    en1 = en1 + en_dis(i)/nmax;
end
    en2 = 0;
for i = 1:nmax
    en2 = en2 + ( en_dis(i)^2 )/nmax;
end

% calculation of transition rate step 2-2: tarnsition rate

beta = 1/temp;
alpha= sqrt(alpha2_n/arate);

%if (ilcl/(1*1)==ilcl)
% call table(mx,my, idim, mcut, nmax, isx, isy, en_dis, pij, anui, &
ixy, tau0, anu0, alpha, beta)

% isx(idim);
% isy(idim);
% en_dis(idim);
% pij(idim,0:mcut);
% ixy(idim,mcut);
% sum(0:mcut);
% icand(mcut,0:1);
% rdis(mcut,0:1);
% anui(idim)
acx = 0.5*mx;
acy = 0.5*my;

    ia = 0;
    ib = 1;

for imain = 1:nmax
    for idm = 1:mcut
        icand(idm,1) = idm;
        rdis(idm,1) = 5000;
        icand(idm,2) = idm;
        rdis(idm,2) = 5000;
    end
end

```



```

end

% c sourting largest mcut (j in equation 2 prb58,19,1998)
for j = 1: nmax
    ia = -ia + 1;
    ib = -ib + 1;
    if(j==imain)
        for idm = 1:mcut
            icand(idm,ia+1)=icand(idm,ib+1);
            rdis(idm,ia+1)=rdis(idm,ib+1);
        end
    end

    ax = isx(imain)-isx(j);
    ay = isy(imain)-isy(j);
    ax = abs(ax);
    ay = abs(ay);
    if(ax>acx)
        ax = mx - ax;
    end

    if(ay>acy)
        ay = my - ay;
    end
    rr = sqrt( ax^2 + ay^2 );

% c case 1 , rr <_ rdis(1)
    if(rr< rdis(1,ib+1))

        for ir = 2:mcut
            icand(ir,ia+1) = icand(ir-1,ib+1);
            rdis(ir,ia+1) = rdis(ir-1,ib+1);
        end
        icand(1,ia+1) = j;
        rdis(1,ia+1) = rr;
    end
% c case 2 rdis(mcut-1) < rr <_ rdis(mcut)

    if( (rr >= rdis(mcut-1,ib+1))&& (rr<rdis(mcut,ib+1)))
        for ir = 1: mcut-1
            icand(ir,ia+1) = icand(ir,ib+1);
            rdis(ir,ia+1) = rdis(ir,ib+1);
        end
        icand(mcut,ia+1) = j;
        rdis(mcut,ia+1) = rr;
    end

% c case 3 rdis(itry-1) < rr <_ rdis(itry)
    for itry = 2: mcut-1
        if( (rr>= rdis(itry-1,ib+1)) && (rr < rdis(itry,ib+1)))

            for ir = 1:itry-1
                icand(ir,ia+1) = icand(ir,ib+1);
                rdis(ir,ia+1) = rdis(ir,ib+1);
            end
            for ir = itry+1:mcut
                icand(ir,ia+1) = icand(ir-1,ib+1);
                rdis(ir,ia+1) = rdis(ir-1,ib+1);
            end
        end
    end
end

```

```

        end
        icand(itry,ia+1) = j;
        rdis(itry,ia+1) = rr;
    end
end
end

        %calculation of vij
    zz = 1/tau0;
    pij(imain,1) = 1/tau0;

for icut = 1: mcut
    ixy(imain,icut) = icand(icut,ia+1);
    rr = rdis(icut,ia+1);
    en = en_dis(icand(icut,ia+1))- en_dis(imain) ;
if(en>0)
    pij(imain,icut) = anu0*exp(-2*rr/alpha)*exp(-beta*en);
end
    if(en<=0)
        pij(imain,icut) = anu0*exp(-2*rr/alpha);
    end
    zz = zz + pij(imain,icut) ;
end

    asum = 0;
for icut= 1: mcut
    asum = asum + pij(imain,icut)/zz;
    sum(icut) = asum;
end

for icut = 1:mcut
    pij(imain,icut) = sum(icut);
end
    anui(imain) = zz;
end

if(imain==284)
aaa = en_dis(imain);
end

% c start monte calro

for iteration = 1:maxiter
    rans = rand(1);
    rans=nmax*rans + 0.1;
    i = round(rans);
    if i==0;
        i=i+1;
    end

for imonte = 1:maxmonte

% c case 1 recombination
    %rans = rand(1);
    % at = -1*anui(i)*log(rans); % PRB58,19,1988
    at = -(1/anui(i))*log(rans);
    % rans = grnd();
    if(rans <= pij(i,1))
        atime = time(i) + at;

```

```

    aen= - en_dis(i);
    inorm=inorm+1;
    time(i)= 0;
    % callst(idim,nhiste,nhistt,histe,histt,ade,adt,aen,atime,acut_1)
    end

    % c case 2 hopping
    for inum = 1: mcut-1
        if( rans > pij(i,inum)&& rans <= pij(i,inum+1) )
            ij = ixy(i,inum+1);
            time(ij) = time(i) + at;
            i = ij;
        end
    end
end

end

end

for k = 1:nhiste-1
    a_en= -acut_1 + ade*k;
    b_en= -acut_1 + ade*(k+1);
    if(aen>a_en&& aen<=b_en)
        histe(k+1) = histe(k+1) + 1
        ihiste = k
    end
end

end

for j = 1:nhistt-1
    a_en= adt*j;
    b_en= adt*j+1;
    if(atime>a_en && atime<=b_en)
        histt(j+1) = histt(j+1) + 1
        ihistt = j
    end
end

end
for i= 1:nhiste
    energy(i) = -acut_1 + ade*i;
    intensity(i)=histe(i)/inorm;
    plot(energy,intensity)
end

toc;

```

Bibliography

- [1] M. H. Kim, M. F. Schubert, Q. Dai, J. K. Kim, E. F. Schubert, J. Piprek, and Y. Park, "Origin of efficiency drop in GaN-based light-emitting diodes." *Applied Physics Letters*, vol. 91, no. 18, pp. 183507-3, Jan. 2007.
- [2] N. Tansu, H. Zhao, G. Liu, X. H. Li, J. Zhang, H. Tong, and Y. K. Ee, "III-nitride photonics." *Photonics Journal, IEEE*, vol. 2, no. 2, pp. 241-248 Jan. 2010.
- [3] G. Liu, J. Zhang, X.-H. Li, G. S. Huang, T. Paskova, K. R. Evans, H. Zhao, and N. Tansu, "Metalorganic vapor phase epitaxy and characterizations of nearly-lattice-matched AlInN alloys on GaN/sapphire templates and free-standing GaN substrates." *Journal of Crystal Growth*, vol. 340, no. 1, pp. 66-73, Feb. 2012.
- [4] Y. F. Wu, A. Saxler, M. Moore, R. P. Smith, S. Sheppard, P. M. Chavarkar, T. Wisleder, U. K. Mishra, and P. Parikh, "30-W/mm GaN HEMTs by field plate optimization." *Electron Device Letters, IEEE*, vol. 25, no. 3, pp. 117-119, March. 2004).
- [5] K. Kazlauskas, G. Tamulaitis, P. Pobedinskas, A. Žukauskas, M. Springis, Chi-Feng Huang, Yung-Chen Cheng, and C. C. Yang. "Exciton hopping in $\text{In}_x\text{Ga}_{1-x}\text{N}$ multiple quantum wells." *Physical Review B*, vol. 71, no. 8, pp. 085306-4, May. 2005.
- [6] S. Nakamura, M. Senoh, S. I. Nagahama, N. Iwasa, T. Yamada, T. Matsushita, Y. Sugimoto, and H. Kiyoku. "High-power, long-lifetime InGaN multi-quantum-well-structure laser diodes." *Japanese journal of applied physics*, vol. 36, no. 8B, pp. L1059, Jan. 1997.
- [7] G. Franssen, T. Suski, M. Kryśko, A. Khachapuridze, R. Kudrawiec, J. Misiewicz, A. Kamińska, E. Feltin, and N. Grandjean, "Built-in electric field and large Stokes shift in near-lattice-matched GaN/AlInN quantum wells." *Applied Physics Letters*, vol. 92, no. 20, pp. 201901-3, Feb. 2008.
- [8] R. Butté, J. F. Carlin, E. Feltin, M. Gonschorek, S. Nicolay, G. Christmann, D. Simeonov, A. Castiglia, J. Dorsaz, H. J. Buehlmann, and S. Christopoulos "Current status of AlInN layers lattice-matched to GaN for photonics and electronics." *Journal of Physics D: Applied Physics*, vol. 40, no. 20, pp. 6328-4, May. 2007.
- [9] O. Ambacher, "Growth and applications of group III-nitrides." *Journal of Physics D: Applied Physics* vol. 31, no. 20, pp. 2653, Dec. 1998.
- [10] J. Wu, W. Walukiewicz, S. X. Li, R. Armitage, J. C. Ho, E. R. Weber, E. E. Haller, H. Lu, W. J. Schaff, A. Barcz, and R. Jakiela, "Effects of electron concentration on the

- optical absorption edge of InN." *Applied physics letters*, vol. 84, no. 15, pp. 2805-2807, Nov. 2004.
- [11] X. Q. Wang, S. B. Che, Y. Ishitani, and A. Yoshikawa, "Experimental determination of strain-free Raman frequencies and deformation potentials for the E2 high and A1 (LO) modes in hexagonal InN." *Applied physics letters*, vol. 89, no. 17, pp. 1907-3, Oct. 2006.
- [12] B. T. Liou, S. H. Yen, and Y. K. Kuo, *Applied Physics A-Materials Science & Processing* vol. 81, pp. 651, Jan. 2005.
- [13] M. Holtz, T. Prokofyeva, M. Seon, K. Copeland, J. Vanbuskirk, S. Williams, S. Nikishin, V. Tretyakov, and H. Temkin, "Composition dependence of the optical phonon energies in hexagonal $\text{Al}_x\text{Ga}_{1-x}\text{N}$." *Journal of Applied Physics*, vol. 89, no. 12, Aug. 2001.
- [14] G. Popovici and H. Morkoc, in *GaN and Related Materials II*, Edited by S. J. Pearton (Gordon and Breach Science Publishers, Amsterdam, 2000), Chap. 3.
- [15] D. Song, Phonons and optical properties of III-nitride semiconductors, PhD diss., Texas Tech University, 2007.
- [16] Z. H. Wu, A. M. Fischer, F. A. Ponce, W. Lee, J. H. Ryou, J. Limb, D. Yoo, and R. D. Dupuis. "Effect of internal electrostatic fields in InGaN quantum wells on the properties of green light emitting diodes." *Applied Physics Letters*, vol. 91, no. 4, pp. 041915-3, Jul. 2007.
- [17] H. Wang, Z. Ji, S. Qu, G. Wang, Y. Jiang, B. Liu, X. Xu, and H. Mino. "Influence of excitation power and temperature on photoluminescence in InGaN/GaN multiple quantum wells." *Optics express*, vol. 20, no. 4, pp. 3932-3940, Aug. 2012.
- [18] Y. Zhang, R. M. Smith, Y. Hou, B. Xu, Y. Gong, J. Bai, and T. Wang. "Stokes shift in semi-polar (1122) InGaN/GaN multiple quantum wells." *Applied Physics Letters*, vol. 108, no. 3, pp. 031108-4, Jul. 2016.
- [19] M. Monavarian, D. Rosales, B. Gil, N. Izyumskaya, S. Das, Ü. Özgür, H. Morkoç, and V. Avrutin. "Exciton localization in (1122)-oriented semi-polar InGaN multiple quantum wells." In *SPIE OPTO*, pp. 974826-974826. International Society for Optics and Photonics, 2016.
- [20] J. A. Davidson, P. Dawson, T. Wang, T. Sugahara, J. W. Orton, and S. Sakai. "Photoluminescence studies of InGaN/GaN multi-quantum wells." *Semiconductor science and technology*, vol. 15, no. 6, pp. 497-5, Jan. 2000.

- [21] D. W. Parris, M. J. Godfrey, P. Dawson, R. A. Oliver, M. J. Galtrey, M. J. Kappers, and C. J. Humphreys. "Carrier localization mechanisms in $\text{In}_x\text{Ga}_{1-x}\text{N}/\text{GaN}$ quantum wells." *Physical Review B*, vol. 83, no. 11, pp. 115321-3, Jul. 2011.
- [22] T. J. Badcock, P. Dawson, M. J. Davies, M. J. Kappers, FC-P. Massabuau, F. Oehler, R. A. Oliver, and C. J. Humphreys. "Low temperature carrier redistribution dynamics in InGaN/GaN quantum wells." *Journal of Applied Physics*, vol. 115, no. 11, pp. 113505-5, Jul. 2014.
- [23] J.-F. Carlin and M. Ilegems, "High-quality AlInN for high index contrast Bragg mirrors lattice matched to GaN ." *Applied physics letters*, vol. 83, no. 4, pp. 668-670, May. 2003.
- [24] K. Lorenz, N. Franco, E. Alves, I. M. Watson, R. W. Martin, and K. P. O' Donnell, "Anomalous ion channeling in AlInN/GaN bilayers: determination of the strain state." *Physical review letters* vol. 97, no. 8, pp. 085501-4, Jan. 2006.
- [25] V. Fiorentini, F. Bernardini, F. Della Salla, A. Di Carlo, and P. Lugli, "Effects of macroscopic polarization in III-V nitride multiple quantum wells." *Physical Review B*, vol. 60, no. 12, pp.8849, Jul. 1999.
- [26] . Akasaki, and H. Amano. "Crystal growth and conductivity control of group III nitride semiconductors and their application to short wavelength light emitters." *Japanese journal of applied physics*, vol. 36, no. 9R, pp. 5393-5, Jan. 1997.
- [27] M. Goano, E. Bellotti, E. Ghillino, G. Ghione, and K. F. Brennan. "Band structure nonlocal pseudopotential calculation of the III-nitride wurtzite phase materials system. Part I. Binary compounds GaN , AlN , and InN ." *Journal of Applied Physics*, vol. 88, no. 11, pp. 6467-6475, Jan. 2000.
- [28] M. Y. Xie, F. Tasnadi, I. A. Abrikosov, L. Hultman, and V. Darakchieva. "Elastic constants, composition, and piezoelectric polarization in $\text{In}_x\text{Al}_{1-x}\text{N}$: From ab initio calculations to experimental implications for the applicability of Vegard's rule." *Physical Review B*, vol. 86, no. 15, pp. 155310-4, Jan. 2012.
- [29] B. Rezaei, A. Asgari, and M. Kalafi. "Electronic band structure pseudopotential calculation of wurtzite III-nitride materials." *Physica B: Condensed Matter*, vol. 371, no. 1, pp. 107-111, March. 2006.
- [30] M. Fox, *Optical Properties of Solids*, Oxford Master Series in Physics (Oxford University Press, 2008), pp.131.

- [31] D. Fritsch, H. Schmidt, and M. Grundmann. "Band-structure pseudopotential calculation of zinc-blende and wurtzite AlN, GaN, and InN." *Physical Review, B* vol. 67, no. 23, pp. 235205-4, Apr. 2003.
- [32] A. Beloufa, Z. Bensaad, B. A. Soudini, N. Sekkal, A. Bensaad, and H. Abid. "Ab initio Calculations of Structural and Electronic Properties of the III-V Nitride Compounds and their Applications to Laser Diodes." *American Journal of Materials Science*, vol. 1, no. 1, pp. 45-51, Jul. 2011.
- [33] H. Morko, *Nitride Semiconductors and Devices* (1999).
- [34] H. X. Jiang, J. Y. Lin, and W. W. Chow, in *III-Nitride Semiconductors: Optical Properties I*, Edited by M. O. Manasreh and H. X. Jiang (Taylor & Francis Books, Inc., New York, 2002), Chap. 2.
- [35] S. J. Xu, W. Liu, and M. F. Li. "Effect of temperature on longitudinal optical phonon-assisted exciton luminescence in heteroepitaxial GaN layer." *Applied Physics Letters*, vol. 77, no. 21, pp. 3376-3, June. 2000.
- [36] D. Y. Song, M. Basavaraj, S. A. Nikishin, M. Holtz, V. Soukhoveev, A. Usikov, and V. Dmitriev, "The influence of phonons on the optical properties of GaN." *Journal of applied physics*, vol. 100, no. 11, pp. 113504, May. 2006.
- [37] S. W. Koch, M. Kira, G. Khitrova, and H. M. Gibbs. "Semiconductor excitons in new light." *Nature materials*, vol. 5, no. 7, pp. 523-531, Oct. 2006.
- [38] K. Itoh, T. Kawamoto, H. Amano, K. Hiramatsu, and I. Akasaki. "Metalorganic vapor phase epitaxial growth and properties of GaN/Al_{0.1}Ga_{0.9}N layered structures." *Japanese journal of applied physics*, vol. 30, no. 9R, pp.1924-5, June. 1991.
- [39] I. Akasaki, H. Amano, K. Itoh, N. Koide & K. Manabe, "GaN-based UV/blue light emitting devices." *International Physics Conference Series*, vol. 129, pp. 851-5, Jan.1992.
- [40] S. Nakamura, and T. Mukai. "High-quality InGaN films grown on GaN films." *Japanese journal of applied physics*, vol. 31, no. 10B, pp. L1457-5, Jul. 1992.
- [41] S. Nakamura, T. Mukai, M. Senoh, S. Nagahama, and N. Iwasa. "In_xGa_{1-x}N/In_yGa_{1-y}N super-lattices grown on GaN films." *Journal of applied physics*, vol. 74, no. 6, pp. 3911-3915, Jul. 1993.
- [42] S. Nakamura, T. Mukai, and M. Senoh. "Candela-class high-brightness InGaN/AlGaIn double-heterostructure blue-light-emitting diodes." *Applied Physics Letters*, vol. 64, no. 13, pp. 1687-1689, March. 1994.

- [43] T. M. Smeeton, M. J. Kappers, J. S. Barnard, M. E. Vickers, and C. J. Humphreys. "Electron-beam-induced strain within InGaN quantum wells: False indium "cluster" detection in the transmission electron microscope." *Applied Physics Letters*, vol. 83, no. 26, pp. 5419-5421, Jan. 2003.
- [44] D. R. Vij, in *Luminescence of Solids* (Plenum Press, New York, 1998).
- [45] M. Baeumler and W. Jantz, in *Microprobe Characterizations of Optoelectronic Materials*, Edited by J. Jimenez (Taylor & Francis Books, INC., New York, 2003), Vol. Microprobe Characterizations of Optoelectronic Materials, Chap. 1.
- [46] M. Kira, and S. W. Koch. *Semiconductor quantum optics*. Cambridge University Press, 2011.
- [47] H. Haug, and S. W. Koch. *Quantum theory of the optical and electronic properties of semiconductors*. vol. 5. Singapore: World scientific, 1990.
- [48] J. Lähnemann, U. Jahn, O. Brandt, T. Flissikowski, P. Dogan, and H. T. Grahn. "Luminescence associated with stacking faults in GaN." *Journal of Physics D: Applied Physics*, vol. 47, no. 42, pp. 423001-5, Dec. 2014.
- [49] S. D. Baranovskii, R. Eichmann, and P. Thomas. "Temperature-dependent exciton luminescence in quantum wells by computer simulation." *Physical Review B*, vol. 58, no. 19, pp. 13081-4, July. 1998.
- [50] <http://www2.mpip-mainz.mpg.de/groups/laquai/Research/Transient%20PL/?lang=en>
- [51] D. Monroe, "Hopping exponential band tails," *Physical Review Letters B*, vol. 54, no. 2, pp. 146–149, Feb. 1985.
- [52] M. Grünewald, B. Movaghar, B. Pohlmann, and D. Würtz, "Hopping theory of band-tail relaxation in disordered semiconductors," *Physical Review B : Condens. Matter*, vol. 32, no. 12, pp. 8191–8196, Aug. 1985.
- [53] K. Kazlauskas, G. Tamulaitis, A. Žukauskas, M. A. Khan, J. W. Yang, J. Zhang, G. Simin, M. S. Shur, and R. Gaska, "Double-scaled potential profile in a group-III nitride alloy revealed by Monte Carlo simulation of exciton hopping," *Applied Physics Letters*, vol. 83, no. 18, pp. 3722–3724, Jul. 2003.
- [54] M. A. Khan, J. W. Yang, G. Simin, R. Gaska, M. S. Shur, H. C. Loye, G. Tamulaitis, "Lattice and Energy Band Engineering in AlInGaN/Ga Heterostructures." *Applied Physics Letters*, vol. 76, no. 9, pp. 1161-1163, July. 2000.

- [55] G. Tamulaitis, K. Kazlauskas, S. Juršėnas, A. Žukauskas, M. A. Khan, J. W. Yang, J. Zhang, G. Simin, M. S. Shur, and R. Gaska. "Optical bandgap formation in AlInGaN alloys." *Applied Physics Letters*, vol. 77, no. 14, pp. 2136-2138, May. 2000.
- [56] P. Renwick, "Improving the Performance of III-Nitride Emitters by Nanostructure Fabrication and Surface Plasmon Coupling." PhD diss., University of Sheffield, 2013.
- [57] M. Fox, *Optical Properties of Solids*, Oxford Master Series in Physics (Oxford University Press, page 131, 2008).
- [58] Y. Taniyasu, M. Kasu, and T. Makimoto. "An aluminium nitride light-emitting diode with a wavelength of 210 nanometres." *Nature*, vol. 441, no. 7091, pp. 325-328, Jul. 2006.
- [59] H. Mathieu, P. Lefebvre, and P. Christol. "Simple analytical method for calculating exciton binding energies in semiconductor quantum wells." *Physical Review B*, vol. 46, no. 7, pp. 4092-4, Jan. 1992.
- [60] A. Miller, and E. Abrahams. "Impurity conduction at low concentrations." *Physical Review*, vol. 120, no. 3, pp. 745-4, May. 1960.
- [61] M. Baranowski, R. Kudrawiec, J. Misiewicz, H. Turski, and C. Skierbiszewski, "Photoluminescence characterization of InGaN/InGaN quantum wells grown by plasma-assisted molecular beam epitaxy: Impact of nitrogen and gallium fluxes." *physica status solidi (b)*, vol. 252, no. 5, pp. 983-988, May. 2015.
- [62] M. H. Kalos, and P. A. Whitlock. *Monte Carlo methods*. John Wiley & Sons, 2008.
- [63] M. Silver, G. Schoenherr, and H. Baessler. "Dispersive hopping transport from an exponential energy distribution of sites." *Physical Review Letters*, vol. 48, no. 5, pp. 352-4, Feb. 1982.
- [64] Y. Jiang, Y. Li, Y. Li, Z. Deng, T. Lu, Z. Ma, P. Zuo, L. Dai, L. Wang, H. Jia, W. Wang. "Realization of high-luminous-efficiency InGaN light-emitting diodes in the "green gap" range." *Scientific reports*, vol. 5, May. 2015.
- [65] T. Lu, Z. Ma, C. Du, Y. Fang, H. Wu, Y. Jiang, L. Wang et al. "Temperature-dependent photoluminescence in light-emitting diodes." *Scientific reports*, vol. 4, pp., Aug. 2014.
- [66] M. A. Sousa, T. C. Esteves, N. B. Sedrine, J. Rodrigues, M. B. Lourenço, A. R. Cubero, E. Alves et al. "Luminescence studies on green emitting InGaN/GaN MQWs implanted with nitrogen." *Scientific reports*, vol. 5, pp., Apr. 2015.

- [67] E. Berkowicz, D. Gershoni, G. Bahir, E. Lakin, D. Shilo, E. Zolotoyabko, A. C. Abare, S. Pi Denbaars, and L. A. Coldren. "Measured and calculated radiative lifetime and optical absorption of $\text{In}_x\text{Ga}_{1-x}\text{N}/\text{GaN}$ quantum structures." *Phys. Rev. B*, vol. 61, pp. 10994-6, July. 2000.
- [68] Y. H. Cho, G. H. Gainer, A. J. Fischer, J. J. Song, S. Keller, U. K. Mishra, and S. P. DenBaars. "'S-shaped' temperature-dependent emission shift and carrier dynamics in InGaN/GaN multiple quantum wells." *Appl. Phys. Lett.* **73**, pp. 1370-3, Feb. 1998.
- [69] A. Mohanta, S. F. Wang, T. F. Young, P. H. Yeh, D. C. Ling, M. E. Lee, and D. J. Jang. "Observation of weak carrier localization in green emitting InGaN/GaN multi-quantum well structure." *Journal of Applied Physics*, vol. 117, no. 14, pp. 144503-6, Jan. 2015.
- [70] E. Liu, D. G. Zhao, D. S. Jiang, P. Chen, Z. S. Liu, J. J. Zhu, M. Shi et al. "Temperature dependence of photoluminescence spectra for green light emission from InGaN/GaN multiple wells." *Optics express*, vol. 23, no. 12, pp. 15935-15943, Dec. 2015.
- [71] W. Walukiewicz, S. X. Li, J. Wu, K. M. Yu, J. WIII Ager, E. E. Haller, Hai Lu, and William J. Schaff. "Optical properties and electronic structure of InN and In -rich group III-nitride alloys." *Journal of Crystal Growth*, vol. 269, no. 1, pp. 119-127, Aug. 2004.
- [72] B. D. Don, K. Kohary, E. Tsitsishvili, H. Kalt, S. D. Baranovskii, and P. Thomas. "Quantitative interpretation of the phonon-assisted redistribution processes of excitons in $\text{Zn}_{1-x}\text{Cd}_x\text{Se}$ quantum islands." *Physical Review B*, vol. 69, no. 4, pp. 045318-6, Jan. 2004).